geologica acta

Citation: García-Penas, Á., Zamora, S., Moreno-Bedmar, J.A., Calvín, P., Aurell, M., 2025. Latest Barremian - early Aptian chronostratigraphy and sedimentary evolution of the northwestern Maestrat Basin. Geologica Acta, 23.1, 1-23, I-III.

Online ISSN: 1696-5728 DOI: 10.1344/GeologicaActa2025.23.1

Latest Barremian - early Aptian chronostratigraphy and sedimentary evolution of the northwestern Maestrat Basin

Álvaro García-Penas[1] Samuel Zamora[2] Josep A. Moreno-Bedmar[3] Pablo Calvín[2] Marcos Aurell[1]

[1]Dpto. Ciencias de la Tierra-IUCA, Universidad Zaragoza
50009 Zaragoza (Spain). García-Penas E-mail: alvarogpenas@gmail.com Aurell E-mail: maurell@unizar.es

[2]Instituto Geológico y Minero de España (IGME-CSIC)
Avda. Montañana 1005, 50059 Zaragoza, Spain. Zamora E-mail: s.zamora@igme.es Calvin E-mail: p.calvin@igme.es

[3]Instituto de Geología, Universidad Nacional Autónoma de México
Ciudad Universitaria, Coyoacán, 04510 Ciudad de México, Mexico. Moreno-Bedmar E-mail: josepamb@geologia.unam.mx

ABSTRACT

Some aspects on the age and correlation of the upper Barremian-lower Aptian stratigraphic units of the NW Maestrat Basin were uncertain prior to this study, due to the differing lithostratigraphy of the marginal Oliete subbasin compared to the more depocentral Galve and Morella subbasins. New magnetostratigraphic, ammonite and sedimentological data presented in this study refine the age and sequence stratigraphy of the upper Barremian-lower Aptian succession, enabling a direct and precise correlation across these subbasins. Three third-order TR sequences are identified. The lower boundary of Sequence 1 corresponds to a transgressive surface found on top of the continental red beds of the lower Morella Fm. These beds are equivalent in age to the continental succession of the upper Blesa Fm. (Fm. (Oliete subbasin). The boundary between the M1 and M0r magnetozones (latest Barremian) is found above this surface, in the lower part of the Alacón Fm. Sequence 1 includes the lower part of the Alacón Fm., which passes basinwards to the upper Morella and Xert formations. Sequence 2 corresponds to the upper part of the Alacón Fm and basinwards to the Cap de Vinyet and Barra de Morella members of the Forcall Fm. The boundary between the M0r and C34n magnetozones (earliest Aptian) is found towards the lowermost part of Sequence 2. Sequence 3 includes the Josa Fm and its offshore equivalents, the Morella la Vella Mb. and the Villarroya de los Pinares Fm. Additionally, the overall facies distribution in successive depositional stages is reconstructed, describing the lateral transition from marginal protected to open marine areas. The improved chronostratigraphic framework presented here will enable more accurate correlations with other subbasins of the Maestrat Basin, and the reconstructed sedimentary evolution may be useful for the interpretation of other Lower Cretaceous successions of the Tethys.

KEYWORDS **Cretaceous. Iberia. Magnetostratigraphy. Ammonites. Sequence stratigraphy.**

INTRODUCTION

The Maestrat Basin developed in the eastern Iberian Plate during the Late Jurassic-Early Cretaceous reactivation of the Mesozoic Central Iberian rift system. The up to 4km-thick synrift sedimentary succession recorded in this basin includes continental to marine carbonate and siliciclastic rocks. The lithostratigraphy of this succession was first defined by Canérot (1974) and Canérot *et al.*

(1982). Later, the sequence stratigraphy analysis carried out by Salas (1987) provided a genetic approach, which brough significant advances to the understanding of the stratigraphic framework. The tectonosedimentary evolution of the Maestrat Basin was also defined in successive contributions, identifying the main extensional tectonic structures involved in the development of subbasins (Salas and Casas, 1993; Salas and Guimerà, 1996; Salas *et al.*, 1995, 2001). The evolution of this basin includes two stages of rifting with rapid tectonic subsidence during the Kimmeridgian-Berriasian and Barremian-mid Albian, which are separated by a period of relative tectonic quiescence spanning most of the Valanginian and Hauterivian (*e.g.* Aurell *et al.*, 2019a; Martín-Chivelet *et al.*, 2019; Salas *et al.*, 2001).

The upper Barremian to Aptian successions deposited during the second rifting stage are well represented in the Morella, Galve and Oliete subbasins (northwestern Maestrat Basin) analysed here (Fig. 1A). In the Oliete subbasin, early contributions by Murat (1983), Vennin *et al.* (1993), and Soria *et al.* (1994) provided the basis for the facies and sequence stratigraphy analysis of Aurell *et al.* (2018) and García-Penas *et al.* (2022, 2024). In the Galve subbasin, further stratigraphical and sedimentological analysis in these successions resulted in a detailed knowledge of the sequence architecture and facies transition from coastal to open-marine areas (Bover-Arnal *et al.*, 2009, 2010, 2012, 2015, 2016, 2022, 2024; Embry *et al.*, 2010; Peropadre, 2012; Peropadre *et al.*, 2013; Vennin and Aurell, 2001). Moreover, the analysis of the lower Aptian of the southern area of the Morella subbasin largely contributed to establish a precise ammonite stratigraphy of the Maestrat Basin, and provided the identification and time calibration of the Ocean Anoxic Event (OAE) 1a (Bover-Arnal *et al.*, 2016; García *et al.*, 2014; Moreno-Bedmar *et al.*, 2009, 2010a). The sequence stratigraphy studies of Bover-Arnal *et al.* (2014) and Bover-Arnal and Salas (2019) in the Aptian carbonate platforms exposed in the southeastern area of the Morella subbasin are also relevant. In contrast, since the regional works of Canérot (1974) and Salas (1987), the extensive area spanning the northern, central, and western areas of the Morella subbasin remained understudied. This is a key sector of the Maestrat Basin which encompasses the linkage area between the Oliete, Galve and southern Morella subbasins. Therefore, the present work aims to fill this gap of knowledge with the analysis and correlation of several key outcrops distributed across these poorly explored marginal areas of the Morella subbasin.

The main objective of this work is to integrate new data with previously published information to understand the facies evolution and sequence stratigraphy of the uppermost Barremian-lower Aptian successions of the northwestern Maestrat Basin, including the Oliete, Morella, and Galve subbasins. To reach this objective and to support the proposed correlation we have employed a multidisciplinary approach, integrating biostratigraphy (ammonites), magnetostratigraphy (Alacón Fm., Oliete subbasin), lithostratigraphy, sequence stratigraphy, and isotopic data. These data help to clarify some topics still open to discussion such as the basinwide correlation of the units between the marginal Oliete subbasin and the more open marine southern areas of the Morella and Galve subbasins. Some key chronostratigraphic aspects are also addressed, such as the position of the Barremian-Aptian boundary in the studied successions.

GEOLOGICAL SETTING

The Late Jurassic-Early Cretaceous Iberian rifting phase resulted in the formation of large sedimentary basins in Northeastern Iberia, including the Cameros, Maestrat, Cuenca and Valencia basins (*e.g.* Aurell *et al.*, 2019b; Martín-Chivelet *et al.*, 2019; Salas *et al.*, 2001). The upper Barremian-lower Aptian successions studied here belong to the Oliete, Morella and Galve subbasins (Northwestern Maestrat Basin; Fig. 1A). These subbasins are separated by sedimentary highs. The boundary between the Oliete and Morella subbasins is defined by a SW-NE trending fault system, which resulted in the relative uplift of the Ejulve High (*e.g.* Canérot, 1974; García-Penas *et al.*, 2022). The Morella and Galve subbasins are separated by the NW-SE-trending low-accommodation areas of the Vistabella High (*e.g.* Salas *et al.*, 2001).

In the Galve and Morella subbasins, the studied succession comprises the Morella, Xert, Forcall and Villarroya de los Pinares formations. Bover-Arnal *et al.* (2016) considered this succession as a long-term Transgressive-Regressive (TR) sequence. The lower sequence boundary was located in the middle part of the Morella Fm., on top of a succession dominated by continental red mudstones and sandstones, and was assigned to the mid-late Barremian (upper *Imerites giraudi* Zone). The upper boundary was defined on top of the Villarroya de los Pinares Fm. as a major subaerial unconformity developed at the end of the early Aptian, in the upper *Dufrenoyia furcata* Zone.

In the Oliete subbasin, the studied succession includes the Alacón and Josa formations. These two formations are bounded by major unconformities, which allowed the definition of two long-term TR sequences (García-Penas *et al.*, 2022, 2024; Vennin *et al.*, 1993). The upper boundary of the first sequence is an irregular palaeokarstic surface found on top of Alacón Fm., which has an associated stratigraphic gap of uncertain duration (García-Penas *et al.*, 2022, 2023; Moreno-Bedmar *et al.*, 2010a). Overlying this unconformity, the lower levels of the Josa Fm. and

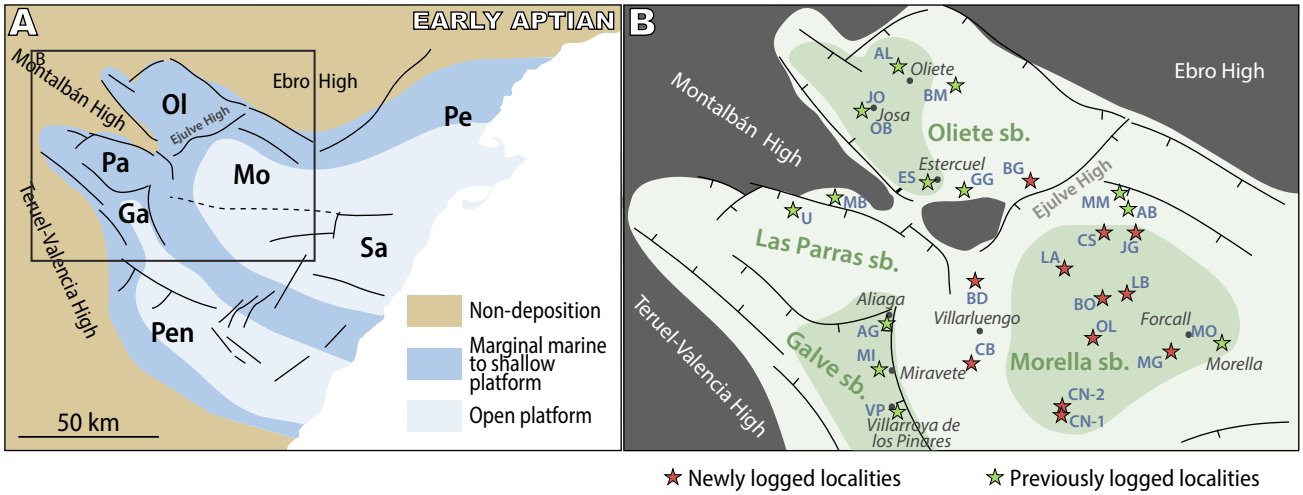

FIGURE 1. A) Palaeogeography of Eastern Iberia during the early Aptian, indicating the distribution of the studied subbasins in the northeastern Maestrat Basin. B) Distribution of the studied outcrops. Oliete subbasin: Alacón-Barranco Emilia-Oliete (AL), Barranco del Moro (BM), Josa-Tejería de Josa (JO), Estercuel (ES), Gargallo (GG), Berge (BG). Morella subbasin: Mas de las Matas (MM), Abenfigo (AB), Jaganta (JG), Castellote (CS), Ladruñán (LA), Bordón (BO), Luco de Bordón-Villores (LB), Olocau del Rey (OL), Barranco de los Degollados (BD), Cañada de Benatanduz (CB), Cantavieja (CV), Forcall-Mola de la Garumba (MG), Morella (MO). Galve subbasin: Aliaga (AG), Miravete-Barranco de las Calzadas (MI), Villarroya de los Pinares (VP). Green shading indicates main subsiding areas. Coordinates of all referenced logs can be consulted in the Supplementary Material.

the equivalent lower levels of the upper member of the Forcall Fm. record a negative carbon isotopic excursion in the upper *Deshayesites forbesi* Zone, which has been attributed to the OAE 1a (Moreno-Bedmar *et al.*, 2009, 2012a). The upper boundary of the second sequence is a major unconformity on top of the Josa Fm., which was considered to be coeval with the unconformity identified on top of the Villarroya de los Pinares Fm. (García-Penas *et al.*, 2023, 2024).

MATERIAL AND METHODS

The new stratigraphic and sedimentological data reported in this work has been acquired by logging new key localities across the Morella subbasin (Fig. 1B). The sections of Barranco de los Degollados (BD) and Cañada de Benatanduz (CB) are located in the western marginal areas of the Morella subbasin. The sections of Ladruñan (LA), Castellote (CA), Jaganta (JG), Bordón (BO), Luco de Bordón-Villores (LB) and Olocau (OL) correspond to the north-central Morella subbasin. In the southern area of the Morella subbasin, new localities have been logged near Cantavieja (CN1 and CN2) and Forcall (Mola de la Garumba, MG). In all these sections, rock samples were collected to characterize the carbonate to mixed carbonate-siliciclastic facies by microscopical analysis of polished slabs and thin sections. Figure 1B also shows the location of ammonite palaeontological sites of Alacón-Barranco Emilia (AL), Tejería de Josa (JO), Miravete-Barranco de las Calzadas (MI), and Morella-Forcall area (MO) reported in Moreno-Bedmar *et al.* (2009, 2010a).

The logs of Alacón (AL) and Barranco del Moro (BM) were sampled for magnetostratigraphic analysis. Fifty-two levels, one meter apart, were sampled in the AL log, where the bedding dips slightly to the south (So: 162/08). This allowed a continuous sampling of the lower and middle part of the Alacón Fm. (sequences A1, A2 and A3 of García-Penas *et al.*, 2022, 2024). Eight kilometres to the west, the entire Alacón Fm. was sampled along a high-dipping bedding series (So: 014/82) in the BM log (Fig. 2B). In the BM log 47 levels were sampled at intervals of approximately 0.5m. Stepwise Thermal (Th) and Alternating Field (AF) demagnetization of the natural remanent magnetization were performed at the Palaeomagnetic Laboratory of the University of Burgos (Spain) using a 755 cryogenic magnetometer (2G) equipped with AF coils and a TD48-DC thermal demagnetizer (ASC scientific). Demagnetization was performed on 87 specimens (52 AL and 35 BM) and AF demagnetization was performed on 31 specimens (2 AL and 29 BM). The characteristic remanent magnetization was calculated per specimen using common paleomagnetic procedures (see Appendix I for more details in the methodological procedures) and these directions were used to calculate the virtual geomagnetic poles (Butler, 1992). Those assigned from quality 1 in Th experiments and quality 1 and 2 in AF experiments were used to establish the local polarity sequence. The quality of thermal CHM directions of each sample can be consulted in Appendix I-Table I.

New ammonites collected in the Josa, Forcall and Benassal formations have allowed to refine the ages of the studied units. Specimens were deposited in the Museo de

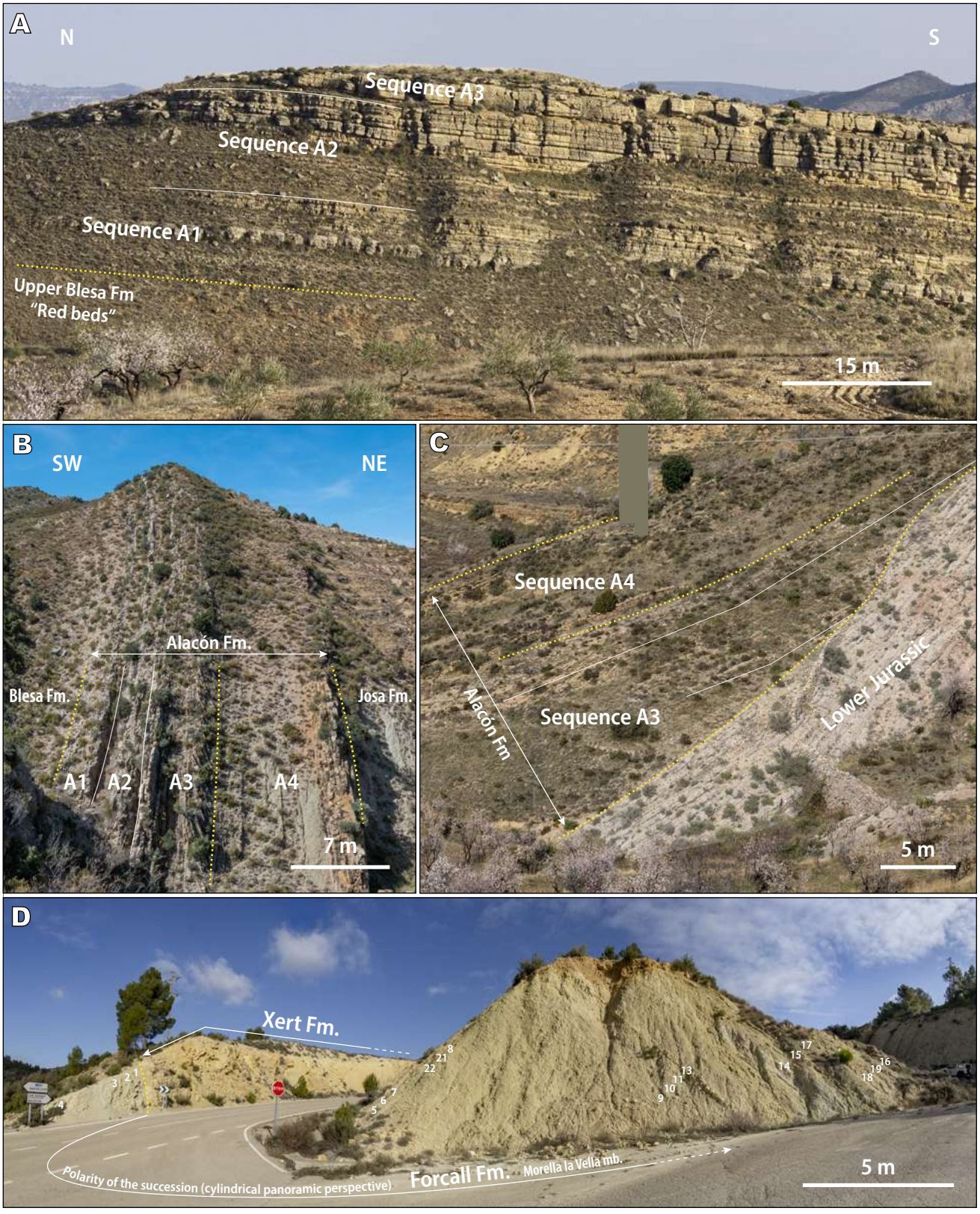

FIGURE 2. A) Panoramic view of a cliff of the Alacón Fm. near the log sampled for the magnetostratigraphic analysis in Alacón (AL), indicating the distribution of sequences A1, A2 and A3 interpreted by García-Penas *et al.* (2022). B) Distribution of sequences A1 to A4 in Barranco del Moro (BM) sampled for the magnetostratigraphic analysis. C) In Gargallo (GG), sequences A3 and A4 (Alacón Fm.) onlap an erosive surface developed over the underlying Jurassic marine carbonates. D) View of the lower Forcall Fm. (Morella la Vella Mb.) in Jaganta (JG). Numbers indicate the distribution of bulk-rock marly to limestone-marly samples collected for isotopic analysis.

Ciencias Naturales de la Universidad de Zaragoza under acronym MPZ. The material was fully prepared using Micro Jack 2 air scribe under a binocular microscope. In some cases, potassium hydroxide (KOH) was used to remove the matrix. Specimens were photographed using a Nikon D7100 camera equipped with AF-S Micro NIKKOR 60 mm objective, following coating with ammonium chloride to enhance contrast. The most recent revision of the Standard Mediterranean Ammonite Zonation (SMAZ) is employed for the ammonite record reported herein (Szives *et al.*, 2024). Over the past two decades, the ammonite zonation of the Aptian stage has undergone significant enhancements, particularly during the lower Aptian timespan in some versions of the SMAZ (Reboulet *et al.*, 2006; Reboulet *et al.*, 2011; Szives *et al.*, 2024). These improvements are based on numerous contributions (*e.g.* Baraboshkin, 2005; Bulot *et al.*, 2014; Dutour, 2005; Frau *et al.*, 2016; García-Mondéjar *et al.*, 2009; Luber *et al.*, 2017; Moreno-Bedmar *et al.*, 2010a; Szives *et al.*, 2023), emphasizing that the Aptian ammonite record reminds under intensive study.

Carbon and oxygen stable isotope analyses were performed on the 20 bulk-rock samples collected in the lower 23m-thick interval of the Forcall Fm. in the Jaganta (JG) log (Fig. 2D). Samples were extracted using a handheld micro-drill. The isotopic analysis of C and O was performed in the Laboratory of Palaeoclimatology and Isotopic Stratigraphy of the Department of Physics and Earth Sciences of the University of Ferrara, using isoFLOW (Elementar©) operating in continuous flow with a PrecisION Isotopic Ratio Mass Spectrometer (IRMS; Elementar©). The $^{13}C/^{12}C$ and $^{18}O/^{16}O$ isotopic ratios were expressed with the δ notation (in ‰ units) relative to V-PDB. The in-house MAQ-1 standard was used for the single-point calibration and two control standards (IAEA 603 and Carrara Marble) were measured to monitor the quality of the analysis. Analytical uncertainties (1σ) for the isotope analyses were in the order of ± 0.1‰ for $\delta^{13}C$ and $\delta^{18}O$.

RESULTS

Magnetostratigraphy of the Alacón Fm.: local polarity sequence and correlation to the Global Polarity Time Scale

Characteristic Remanent Magnetizations (ChRMs, see Appendix II, Fig. I) show a pre-folding behaviour and show antipodal directions (see Appendix II, Fig. II) in agreement with a primary record of the Earth's Magnetic Field. Virtual palaeomagnetic poles (VGPs) were calculated in the two logged sections of the Alacón Fm. in AL and BM from the final ChRM (*e.g.* Butler, 1992). The VGPs, Natural Remanent Magnetization (NRM) and ChRM intensities, unblocking temperatures, and ChRM declinations and inclinations were plotted in a vertical log to establish the local polarity sequence in both profiles (see Fig. 3). The expected palaeolatitude of the VGP, with a mean of 63º for 120-125Ma (Neres *et al.*, 2012), is also shown as well as the 45º cutoff outside of which palaeomagnetic directions are not considered for interpretation.

The AL section (Fig. 3A) shows normal polarities in the first 30m (sequences A1 and A2) derived from ChRM directions and consequent VGPs, defining N1. Reversed polarities are found in the upper part of the section (most of sequence A3, Fig. 3A), defining R1. The lower part in the BM section is also dominated by normal (N1) polarities (Fig. 3B). R1 is well defined between meters 14 to 17 (sequence A3) with paleomagnetic directions from both Th and AF experiments. The upper part of the section is poorly defined, but normal polarities above meter 19 (located in the burrowed and condensed levels found in the lowermost A4 sequence; García-Penas *et al.*, 2022) allow the definition of N2. No difference in the intensities of the NRM and the ChRM or the unblocking temperatures was observed between the normal or reversed polarities sections.

The Local Polarity Sequence (LPS) has been confidently established for the Alacón Fm. in the two studied localities. The available stratigraphic data for the Alacón Fm. (*e.g.* García-Penas *et al.*, 2022) constrain the correlation of the LPS with the Global Polarity Time Scale (Gale *et al.*, 2020). According to the data and interpretations exposed above, the boundary between the M1 and M0r chrons is placed in the mid-lower part of the Alacón Fm. (N1-R1 boundary, Fig. 3), near the boundary between the A2 and A3 sequences of García-Penas *et al.* (2022, 2024). The boundary between the M0r and C34n polarity chrons is found in the lowermost part of A4 sequence (R1-N2 boundary, Fig. 3). The Barremian-Aptian boundary is placed on the boundary between the *Martelites sarasini* and *Deshayesites oglanlensis* zones, which is in turn located in the middle part of M0r chron (Gale *et al.*, 2020; Szives *et al.*, 2024). Accordingly, this stage boundary should be most likely located in the uppermost part of sequence A3.

Ammonite biostratigraphy

The studied successions preserve a rich ammonite record, mainly of lower Aptian taxa (Fig. 4). The seminal work by Moreno-Bedmar *et al.* (2010a) provided a thorough review of previous studies on lower Aptian ammonites from the Maestrat Basin. This work was later enhanced by additional studies (Delanoy *et al.*, 2013, 2022; Forner i Valls and Moreno-Bedmar, 2018; García and Moreno-Bedmar, 2010; García *et al.*, 2014; Grauges

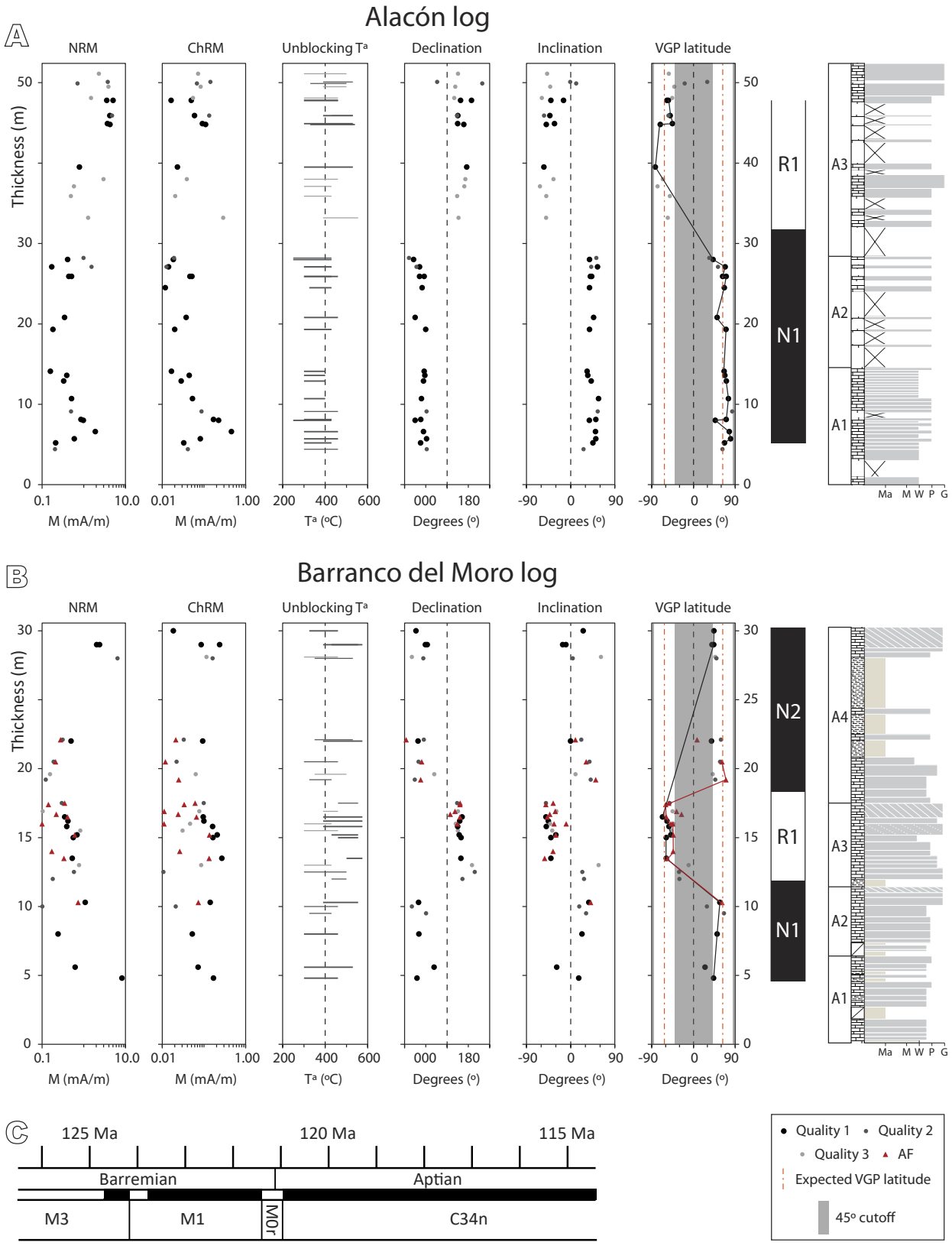

FIGURE 3. Stratigraphic logs and respective palaeomagnetic parameters of the ChRM used to define the different magnetozones and to generate the local polarity sequences for the sampled levels in A) Alacón (AL) and B) Barranco del Moro (BM) sites. C) Polarity time scale around the Barremian-Aptian boundary (Gale *et al.*, 2020; Szives *et al.*, 2024): the local N1, R1 and N2 magnetozones are assigned to the global M1, M0r and C34 magnetozones respectively.

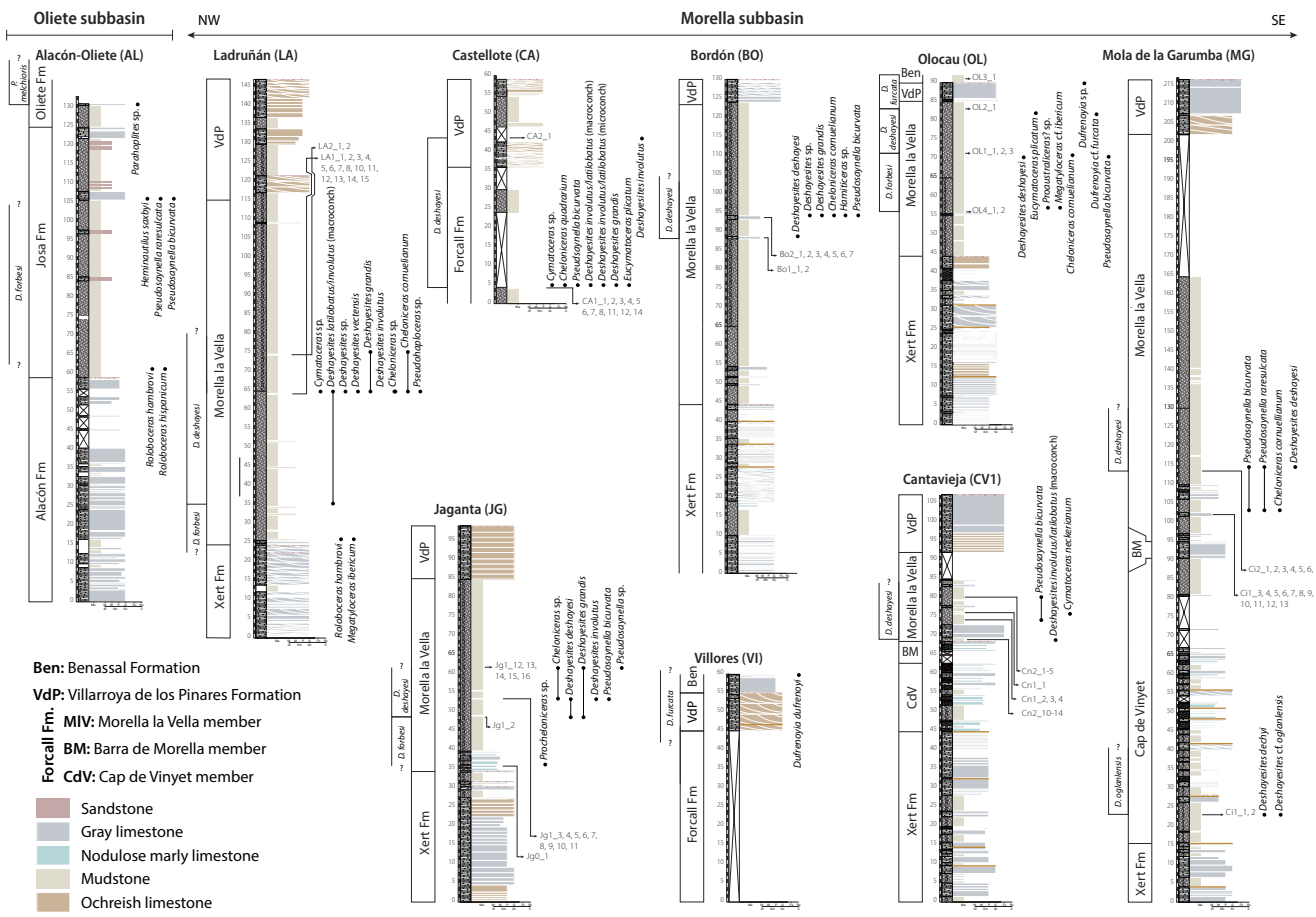

FIGURE 4. Synthetic representation of the logs including new ammonite fossil sites. See Figure 1B for geographical location of the logs.

et al., 2010; Martín-Martín *et al.*, 2013; Moreno-Bedmar *et al.*, 2010b; Moreno-Bedmar *et al.*, 2012a; Moreno-Bedmar *et al.*, 2014). The ammonite biozones identified in this work are described below.

Deshayesites oglanlensis Zone

This ammonite zone is the worst known lower Aptian ammonite zone in the Maestrat Basin due to the scarcity of ammonites and it has only been identified in the Morella subbasin (García *et al.*, 2014; Moreno-Bedmar *et al.*, 2010a). In this study, ammonites of this zone have only been found in the Mola de la Garumba section, in the lower part of the Cap de Vinyet Mb. (Forcall Fm.) (Fig. 4). There, the occurrence of *Deshayesites dechyi* (PAPP, 1907) (Fig. 5A1-2) and *Deshayesites* cf. *oglanlensis* (BOGDANOVA, 1983) (Fig. 5B) likely marks the beginning of the *Deshayesites oglanlensis* Zone, due to its relatively low stratigraphic position compared to the occurrence of *Deshayesites luppovi* (corresponding to the middle/upper part of *Deshayesites oglanlensis* Zone) in the Mas Segura section at about meter 50 of the Forcall Fm. (Moreno-Bedmar *et al.*, 2010a). The discovery of *Deshayesites dechyi* is noteworthy, as it represents the first report of this Russian species in Iberia. The Spanish specimen features a distinctly evolute shell with moderate to low ribbing density, thin and sharp ribs, and poorly developed bullae.

Deshayesites forbesi Zone, Roloboceras hambrovi Subzone

This ammonite zone, particularly its middle/upper part (*Roloboceras hambrovi* Subzone), has a rich ammonite record, present in most subbasins of the Maestrat Basin. The taxa found in this zone include *Roloboceras hambrovi* (FORBES, 1845), *Roloboceras hispanicum* SORNAY AND MARIN, 1972, *Megatyloceras coronatum* (ROUCHADZÉ, 1933), *Megatyloceras ibericum* SORNAY AND MARIN, 1972 (Fig. 5D1-2), *Prochelonicera*s sp., *Pseudosaynella raresulcata* (MICHELIN, 1838) (Fig. 5E1-2), *Pseudosaynella bicurvata* (MICHELIN, 1838) (Fig. 5F1-2), *Proaustraliceras*? sp., and the nautiloid *Heminautilus saxbii* (MORRIS, 1848). Recent taxonomic and biostratigraphic works focusing on the ammonite

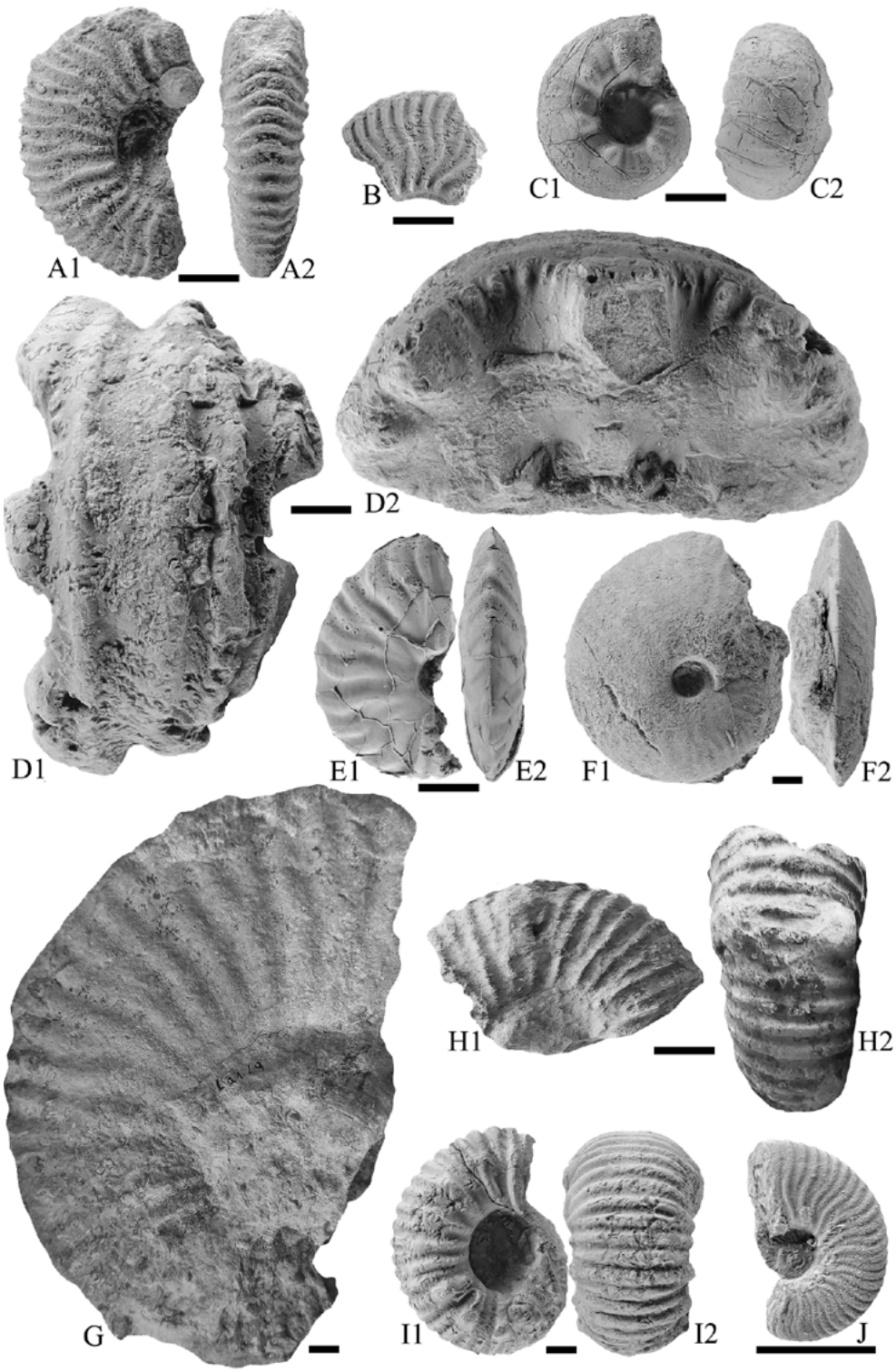

FIGURE 5. A1-2) *Deshayesites dechyi* lateral and ventral views respectively, Mola de la Garumba, sample 1 (Ci1), specimen number MPZ2024/217. B) *Deshayesites* cf. *oglanlensis* lateral view, Mola de la Garumba, sample 1(Ci1), specimen number MPZ2024/218. C1-2) *Roloboceras hispanicum* lateral and ventral views respectively, Oliete, sample 1(Ol1), specimen number Ol1-1. D1-2) *Megatyloceras* cf. *ibericum* ventral and whorl section views respectively, Olocau, sample 4(OL4), specimen number MPZ2024/253. E1-2) *Pseudosaynella raresulcata* lateral and ventral views respectively, Oliete, sample Ol2-1, specimen number Ol2-1. F1-2) *Pseudosaynella bicurvata* lateral and ventral views respectively, Oliete, sample Ol-AM2, specimen number MPZ2024/290. G) *Deshayesites latilobatus/involutus* group (macroconch) lateral view, Ladruñan, sample 1(La1), specimen number MPZ2024/224. H1-2) *Cheloniceras quadrarium* lateral and ventral views respectively, Castellote, sample 1(Ca1), specimen number MPZ2024/245. I1-2) *Cheloniceras cornuelianum* lateral and ventral views respectively, Ladruñan, sample 2 (La2), specimen number MPZ2024/218. J1-2) *Deshayesites grandis l*ateral and ventral views respectively, Ladruñan, sample 1(La1), specimen number MPZ2024/258. Scale bar equal to 1cm.

record of several species of the genera *Roloboceras* and *Megatyloceras* (Delanoy *et al.*, 2022; Frau *et al.*, 2023) have enhanced our understanding of the ammonite assemblage of this subzone.

The *Deshayesites forbesi* Zone, *Roloboceras hambrovi* Subzone, is recognized in the AL section. There, two diagnostic ammonites of the *Roloboceras hambrovi* subzone appear at the lowermost part of the Josa Fm. (Fig. 4). Forty-five meters above, the desmoceratid ammonites *Pseudosaynella raresulcata* and *Pseudosaynella bicurvata* occur with the nautiloid *Heminautilus saxbii*. These desmoceratids have no biostratigraphic value due to their extended ranges (Moreno-Bedmar *et al.*, 2010a; Moreno-Bedmar *et al.*, 2012b), and the same is generally true for Aptian nautiloids. However, this is not the case for the genus *Heminautilus*. *Heminautilus saxbii* disappears in the uppermost part of the *Roloboceras hambrovi* Subzone (Baudouin *et al.*, 2016; Ossó and Moreno-Bedmar, 2020). Therefore, this association in the AL section should be assigned to the *Roloboceras hambrovi* Subzone (Fig. 4). In the LA and OL sections, the *Roloboceras hambrovi* Subzone is characterised by the occurrence of diagnostic ammonites belonging to the genera *Roloboceras* and *Megatyloceras* (Fig. 4). In JG, the *Deshayesites forbesi* Zone is tentatively characterised by the occurrence of *Procheloniceras* sp. This genus ranges from the uppermost Barremian to the lower part of the *Deshayesites forbesi* Zone (Delanoy, 1995, 1997; Ropolo *et al.*, 2008). Considering that ammonites of the *Deshayesites deshayesi* Zone occur about 10 meters above, it seems very likely that *Procheloniceras* sp. may belong to the *Deshayesites forbesi* Zone.

Deshayesites deshayesi Zone

According to our current knowledge, this biozone was never properly recognized in the Oliete subbasin. However, in the Morella and Galve subbasins, this biozone has a rich ammonite record dominated by the subfamily Deshayesitinae. In this study, ammonites of this biozone have been found in the sections of LA, CS (Castellote), BO, OL, MG, JG and CN1 (Fig. 4), all in the Morella subbasin. There, the *Deshayesites deshayesi* Zone is represented by *Deshayesites deshayesi* (D'ORBIGNY, 1841) (Fig. 6B1-2), *Deshayesites latilobatus/involutus* group (macroconch, Fig. 5G), *Deshayesites latilobatus/involutus* group (microconch, Fig. 6C1-2), *Deshayesites involutus* (SPATH, 1930) (Fig. 6A), *Deshayesites vectensis* (SPATH, 1930), *Deshayesites grandis* (SPATH, 1930) (Fig. 5J1-2), *Deshayesites* sp., *Cheloniceras cornuelianum* (D'ORBIGNY, 1841) (Fig. 5I1-2), *Cheloniceras quadrarium* (CASEY, 1962) (Fig. 5H1-2), *Cheloniceras* sp., *Pseudohaploceras* sp., *Pseudosaynella bicurvata*, *Pseudosaynella raresulcata*, *Pseudosaynella* sp., and *Hamiticeras* sp., along with some nautiloids with no biostratigraphic value like *Eucymatoceras plicatum* (FITTON, 1836), *Cymatoceras neckerianum* (PICTET, 1847) and *Cymatoceras* sp. The identification of the *Deshayesites deshayesi* Zone was straightforward because the recognised species of the genus *Deshayesites* (*Deshayesites deshayesi*, *Deshayesites latilobatus/involutus* group, *Deshayesites involutus*, *Deshayesites vectensis*, and *Deshayesites grandis*) have a very short stratigraphic range restricted to this ammonite zone (*e.g.* Moreno-Bedmar *et al.*, 2014).

The discovery in this study of the English species *Cheloniceras quadrarium* (Casey, 1962) is remarkable because it is the first report of this species from the Iberian Peninsula. The Spanish specimen has a quadrangular whorl section, whereas commonly *Cheloniceras* species have a subrectangular whorl section which is wider than high. The Maestrat Basin specimen has gracile ribbing, especially in the flanks, where lateral tuberculation is extremely poorly developed. The characteristics of the Spanish specimen nicely match that of the species described by Casey (1962).

Another remarkable ammonite finding is the specimen illustrated in Figure 6C1-2, identified as a microconch of the *Deshayesites latilobatus/involutus* group. The *Deshayesites latilobatus/involutus* group are, sensu stricto, macroconchs (Moreno-Bedmar *et al.*, 2014). Species such as *Deshayesites geniculatus* Casey, 1964; *Deshayesites vectensis* SPATH, 1930 and *Deshayesites wiltshirei* CASEY, 1964 are microconchs of the *Deshayesites deshayesi* Zone (Moreno-Bedmar *et al.*, 2014). However, these microconchs are highly evolved morphs within the *Deshayesites deshayesi* Zone, implying that their stratigraphic range may span the middle to the upper part of the *Deshayesites deshayesi* Zone. The specimen of Figure 6C1-2 is a quite evolute *Deshayesites* with robust and sharp ribbing. The ribs are strongly sigmoidal, like in juvenile forms of *Deshayesites involutus*. Secondary ribs follow a slightly irregular pattern: usually, secondary ribs are intercalated one to one between main ribs, but sometimes two secondary ribs can appear between a pair of main ribs (Fig. 6C1). This ammonite fills a gap in our knowledge about the succession of deshayesitid microconchs, because its characteristics fall between those of *Deshayesites forbesi* CASEY, 1961 and those of the evolved microconchs of the *Deshayesites deshayesi* Zone. Owing to its morphological characteristics, this morph probably belongs to the lower part of the *Deshayesites deshayesi* Zone. This specimen also allows us to establish the hitherto unknown microconch of the dimorphic pair *Deshayesites latilobatus/involutus*. The microconch of the *Deshayesites latilobatus/involutus* group is more akin to *Deshayesites forbesi* than to evolved microconchs of the *Deshayesites deshayesi* Zone. However, it can be

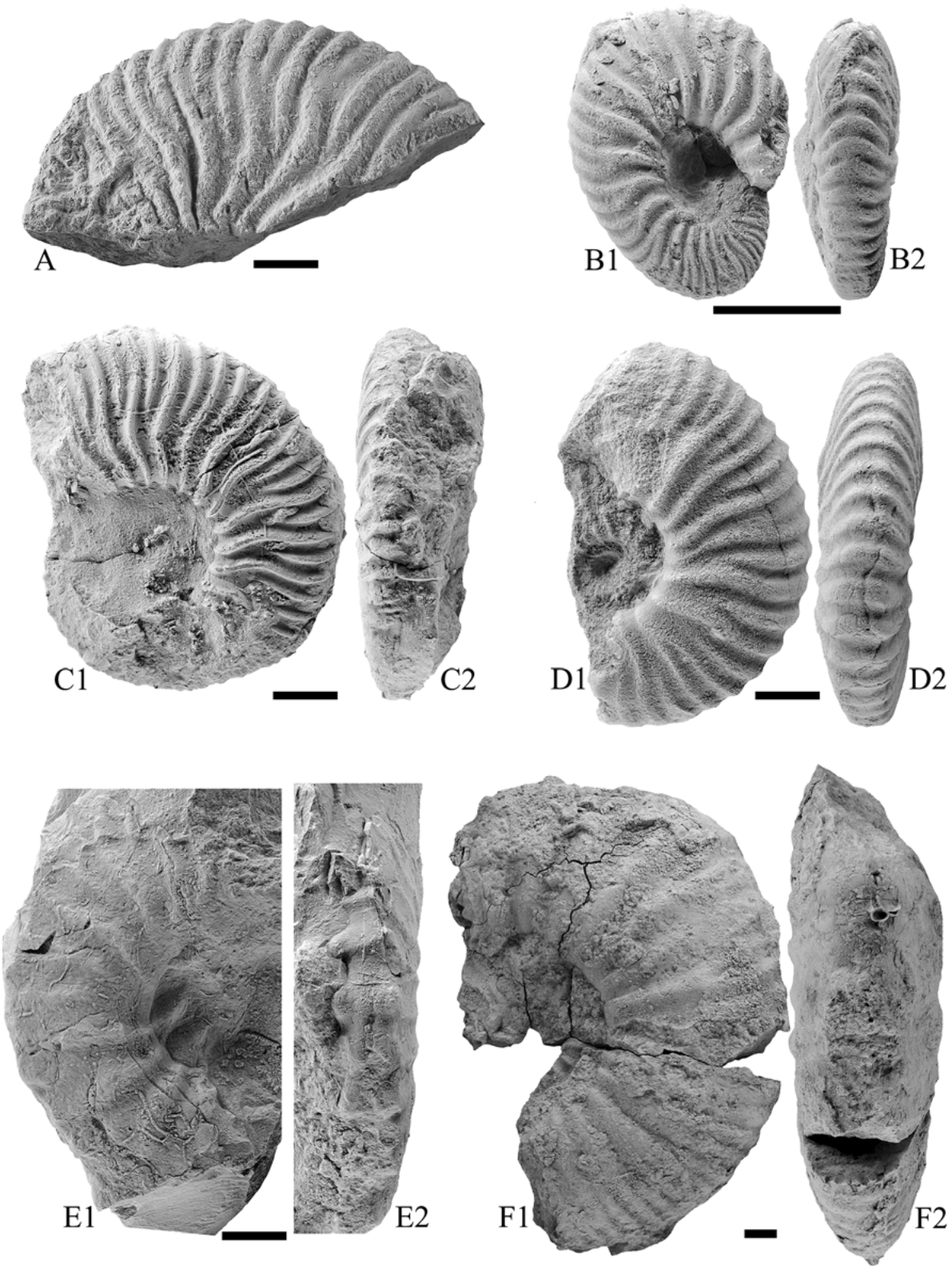

FIGURE 6. A) *Deshayesites involutus* lateral view, Jaganta, sample 1 (Jg1), specimen number MPZ2024/293. B1-2) *Deshayesites deshayesi* lateral and ventral views respectively, Bordón, sample 1 (BO1), specimen number MPZ2024/211. C1-2) *Deshayesites latilobatus/involutus* group (microconch) lateral and ventral views respectively, Castellote, sample 1 (Ca1), specimen number MPZ2024/254. D1-2) *Dufrenoyia* cf. *furcata* lateral and ventral views respectively, Olocau, sample OL1-1, specimen number MPZ2024/209. E1-2) *Dufrenoyia dufrenoyi* lateral and ventral views respectively, Villores, sample 1 (Vi1), specimen number Vi1-1. F1-2) *Parahoplites* sp. lateral and ventral views respectively, Olocau, sample 2, specimen number MPZ2023/191. Scale bar equal to 1cm.

easily distinguished from *Deshayesites forbesi* because this older species has more developed bullae, less sigmoidal ribbing and a clearly more regular pattern of secondary ribbing.

Dufrenoyia furcata Zone

This zone has a scarce record dominated by ammonites of the subfamily Deshayesitinae. In this study, this ammonite zone is represented in the Morella subbasin (OL and VI, Fig. 4) by *Dufrenoyia* cf. *furcata* (SOWERBY, 1836) (Fig. 6D1-2), *Dufrenoyia dufrenoyi* (D'ORBIGNY, 1841) (Fig. 6E1-2), and *Dufrenoyia* sp. Other subbasins, such as the Galve, Penyagolosa, or Perelló subbasins have a considerably better ammonite record of this zone (García *et al.*, 2014; Moreno-Bedmar *et al.*, 2010a). The *Dufrenoyia furcata* Zone is subdivided into two subzones: the older *Dufrenoyia furcata* and the younger *Dufrenoyia dufrenoyi* (Szives *et al.*, 2024). The index species of both subzones are recognized in the OL (uppermost part of the Forcall Fm.) and VI (lowermost part of the Benassal Fm.) sections, respectively (Fig. 4). The age calibration of these two lithostratigraphic units (Fig. 4) supports previous data from Moreno-Bedmar *et al.* (2012a), which was later synthesized in García *et al.* (2014).

Upper Aptian ammonite biostratigraphy

Only one upper Aptian ammonite has been found in the present study. This specimen, classified as *Parahoplites* sp. (Fig. 6F1-2), was recovered from the lower part of the Oliete Fm., in AL (Fig. 4). This genus is restricted to the *Parahoplites melchioris* Zone. García *et al.* (2014) precisely summarized the record of this ammonite zone in the Maestrat Basin based on the presence of several species of the genus *Parahoplites* in the Oliete, Galve, Penyagolosa, and Orpesa subbasins.

ISOTOPIC ANALYSIS OF THE FORCALL FORMATION

In the depocentral areas of the Oliete, Galve and Morella subbasins, a C isotopic excursion attributed to the OAE1a is recorded in the lower part of the Josa Fm., and in the Morella la Vella Mb. of the Forcall Fm. (Moreno-Bedmar *et al.*, 2009). Until now, no isotopic data were available from the northern areas of the Morella subbasin. To check for the potential presence of an isotopic excursion in this area, the lower 23m of the Forcall Fm. were sampled in Jaganta (JG) section (Fig. 2D). The resulting C curve (Fig. 7) only shows a significant positive shift in a 2m-thick level of dark grey marls located above fossil site JG-B (*Deshayesites deshayesi* Zone). The absence of any other isotopic excursion below these fossil sites may indicate that the stratigraphic record of this event is either not represented or highly condensed.

STRATIGRAPHY AND FACIES EVOLUTION

Below we summarize the key stratigraphic and sedimentological information that supports the sequence stratigraphic interpretations and correlations which will be presented and discussed in the following sections. The appendix includes successive figures with representation of the new sections logged in this work. The studied successions are characterised by a wide variety of facies, ranging from pure oolitic grainstones to various matrix-and grain-supported facies, to mudstones. The key aspects of the 15 identified facies (from F1 to F15) are summarized in Table I, Appendix II. Moreover, some of the information reported here is a summary of previously published data and interpretation.

Oliete subbasin

The Alacón Fm. represents the progressive marine flooding of the Oliete subbasin after the sedimentation of the continental upper Blesa Fm. (Aurell *et al.*, 2018; García-Penas *et al.*, 2022). In AL, this unit is represented by alluvial red mudstones and sandstones (Fig. 2A). The 30–60m thick Alacón Fm. shows a wide spectrum of carbonate-dominated coastal to shallow-marine facies deposited in restricted to open-marine conditions (Fig. 2; Appendix III, Figs. III-IV). Its lower part is dominated by limestones with restricted-marine fauna, including mainly ostracods, oysters, serpulids and thin-shelled bivalve and gastropod debris (Facies F16). These materials were deposited in a restricted bay subject to frequent salinity oscillations (see sequences A1-A2; Fig. 2A, B). The middle part of the unit is composed of bioclastic packstones and grainstones with thick-shelled marine bivalves, brachiopods, green algae, bryozoans and coated grains (Facies F6 and F13), which represent the stabilization of normal-marine conditions (sequence A3, Fig. 2A, B). Unusually high localised concentrations of glauconite in this interval indicate stratigraphic condensation (García-Penas *et al.*, 2022). Sequence A3 is topped by an encrusted and iron-rich discontinuity surface. Above this discontinuity, sequence A4 includes a lower c.10-30m thick interval composed of marls and bioturbated marly limestones with orbitolinids, echinoids and other open-marine fauna (Facies F2). This interval is followed by successive m-thick cross-bedded limestones with rounded and well-sorted skeletal grains, peloids, intraclasts, and glauconite (Facies F6). The Alacón Fm. is topped by a prominent palaeokarst (Fig. 8A) developed during a sea level drop that exposed the entire Oliete subbasin subaerially (García-Penas *et al.*, 2022).

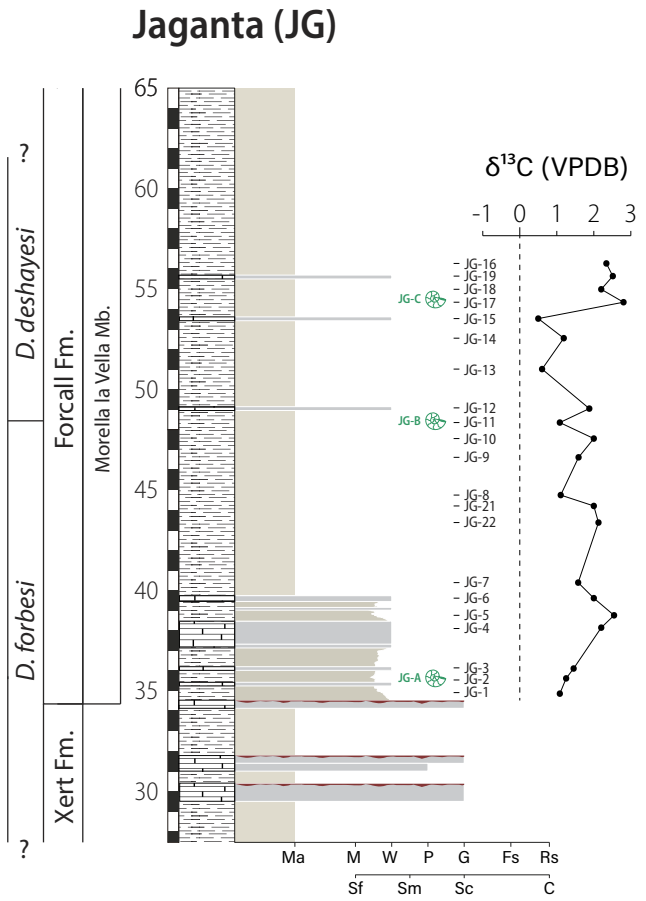

FIGURE 7. C-isotopic curve of the lower Forcall Fm. (Morella la Vella Mb.) in the Jaganta (JG) log.

The thickness of the Alacón Fm. decreases progressively eastwards towards the uplifted Ejulve High (Fig. 1B). In GG, Sequence A3 directly onlaps an erosive surface with abundant *Trypanites* developed over the underlying Jurassic marine carbonates (Fig. 2C). In BG, the 10m-thick Alacón Fm. rests directly on an angular unconformity overlying tilted and eroded Jurassic rocks (see fig. 12C in García-Penas *et al.*, 2024). There, the unit consists of successive planar cross-bedded sets of bioclastic grainstones, which were assigned to sequence A4.

Overlying the paleokarst surface on top of the Alacón Fm., the 20–65m-thick Josa Fm. mostly consist of mudstones and marls with hummocky cross-laminated sandstone interbeds (Facies F1), deposited in a prodelta environment (García-Penas *et al.*, 2024). In JO and AL, a lower c.10m-thick interval records a carbon isotopic excursion related to the OAE 1a event (Moreno-Bedmar *et al.*, 2009). Above this interval, the long-term coarsening upwards regressive trend of most of the Josa Fm. is marked by a transition from prodelta deposits to poorly-to-well lithified sandstones and bioclastic sandy limestones deposited in freshwater-influenced delta front and littoral environments (García-Penas *et al.*, 2024).

The Josa Fm. is topped by an irregular, iron-encrusted palaeokarst which, in turn, is sharply overlain by mud-supported oyster floatstones of the Oliete Fm. (García-Penas *et al.*, 2024; Vennin *et al.*, 1993). An ammonite of the *Parahoplites melchioris* Zone was found immediately above this unconformity (Fig. 4) suggesting that a significant sedimentary gap is associated with the unconformity bounding the Josa and Oliete formations.

Northern and Central Morella subbasin

New stratigraphic and sedimentological information of the northern and central part of the Morella subbasin has been compiled in the key localities of Ladruñán (LA), Castellote (CS), Jaganta (JG), Bordón (BO), Luco de Bordón-Villores (LB) and Olocau (OL) (Appendix III-Fig. V). Throughout this area, a transgressive surface in the middle part of the Morella Fm. separates a lower interval with continental red mudstones, and an upper interval dominated by a grey coastal terrigenous facies (Fig. 9A, B). These coastal facies progressively grade upward to the shallow marine carbonates of the Xert Fm.

The Xert Fm. consists of two limestone-dominated lithological intervals, separated by a c.10 m-thick marlstone interval including abundant orbitolinids and echinoids (see informal division into lower and upper Xert Fm. in Fig. 9). In all the logged localities, the lower Xert Fm. is bounded on top by a Fe-enriched discontinuity surface. This surface is sharply overlain by the orbitolinid marls of the upper Xert Fm., which pass gradually to an upper limestone-dominated interval.

In LA, the lower Xert Fm. (Fig. 9A) is dominated by irregularly bedded skeletal (oyster-rich) sandy limestones (facies F11). The upper Xert Fm. corresponds to a c.25m-thick succession comprising a lower marl-dominated interval followed by successive m-thick planar-cross bedded sets (facies F6). In JG, the upper Xert Fm. consists of grain-supported skeletal-intraclastic facies (facies F6 and F9), with local cross-bedding and dolomitised intervals. In OC, the lower Xert Fm. corresponds to oyster-rich limestones (facies F11), which grade upwards into cross-bedded skeletal packstones and grainstones with glauconite (facies F6). There, the upper Xert Fm. includes a 44m-thick succession of skeletal and oolitic packstones and grainstones (facies F7 and F8), frequently with large-scale planar cross-bedding (Fig. 9C). In BO, the upper Xert Fm. is 26m-thick and comprises peloidal-bioclastic grainstones with abundant and diverse benthic foraminifera (facies F6, F7, F8, F13).

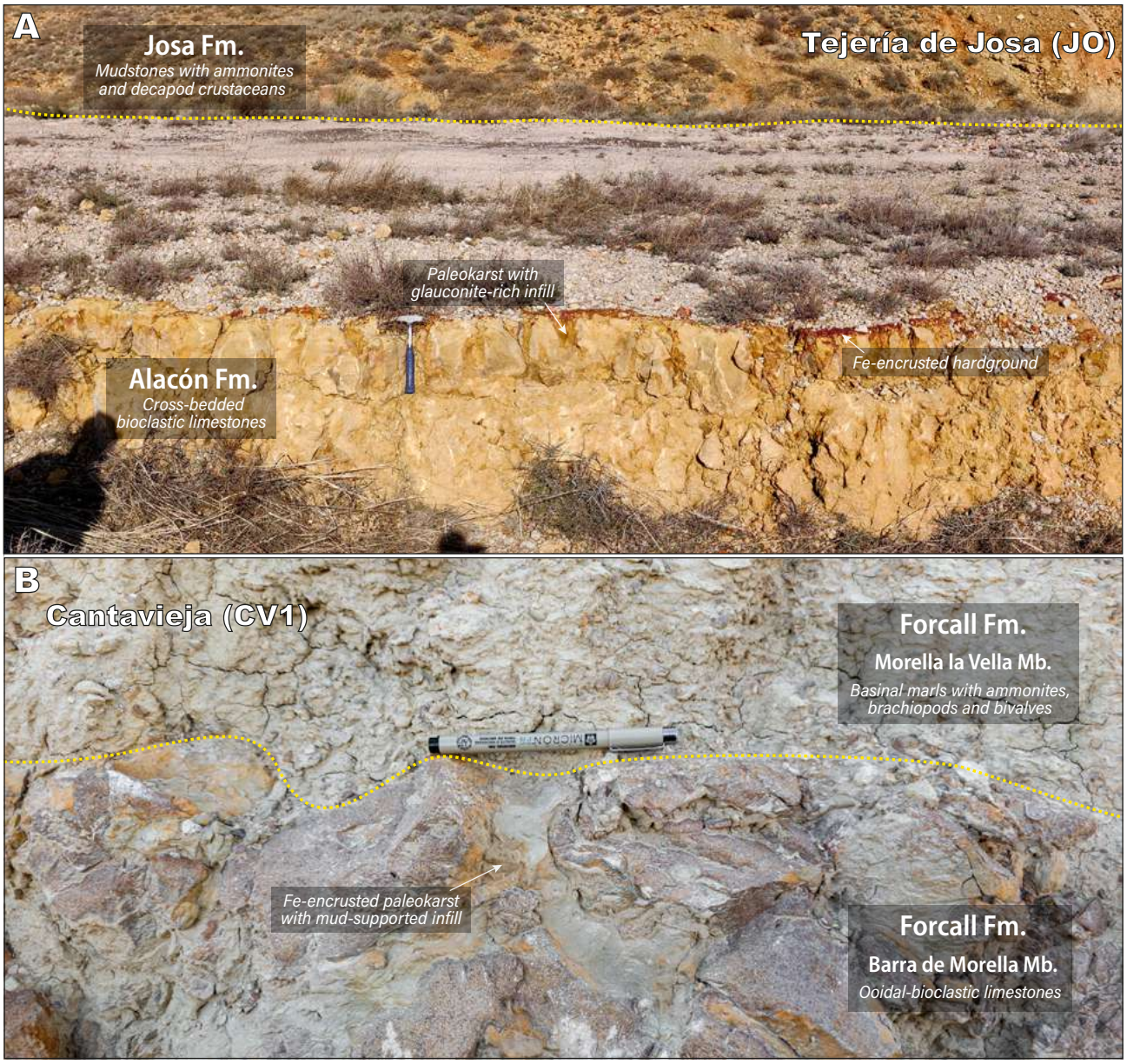

FIGURE 8. A) View of the paleokarst topping the Alacón Fm. in Josa (JO). The top of the bed is mostly covered in gray crushed aggregate of an old road. B) Detail view of the paleokarsts topping the Barra de Morella mb of the Forcall Fm. in Cantavieja (CV1).

Data obtained from the key localities described above, combined with field observations at other intermediate control points, demonstrate the progressive lateral facies change between the upper Xert Fm. (consisting of orbitolinid-rich marls grading upward to grain-supported limestones) and the lower and middle members of the Forcall Fm. (*i.e.* the marls of the Cap de Vinyet Mb. and the skeletal-ooidal limestones of the Barra de Morella Mb.). These two members are well differentiated as independently mappable lithostratigraphic units in the depocentral areas of the Southern Morella subbasin. However, in the marginal Northern Morella subbasin (*e.g.* LA, BO), the equivalent succession (*i.e.* upper Xert Fm.) is not differentiable from the lower Xert Fm. at cartographic scale.

In the Northern Morella subbasin, the discontinuity topping the upper Xert Fm. is an irregular and encrusted surface. Above this discontinuity, the lowermost Forcall Fm. shows the local presence of successive burrowed irregular skeletal beds, which has yielded ammonites of the *Deshayesites forbesi* Zone (JG and LA Fig. 4). Above this interval, a 50-100m thick a marl-dominated succession includes abundant benthic fossils, in particular brachiopods

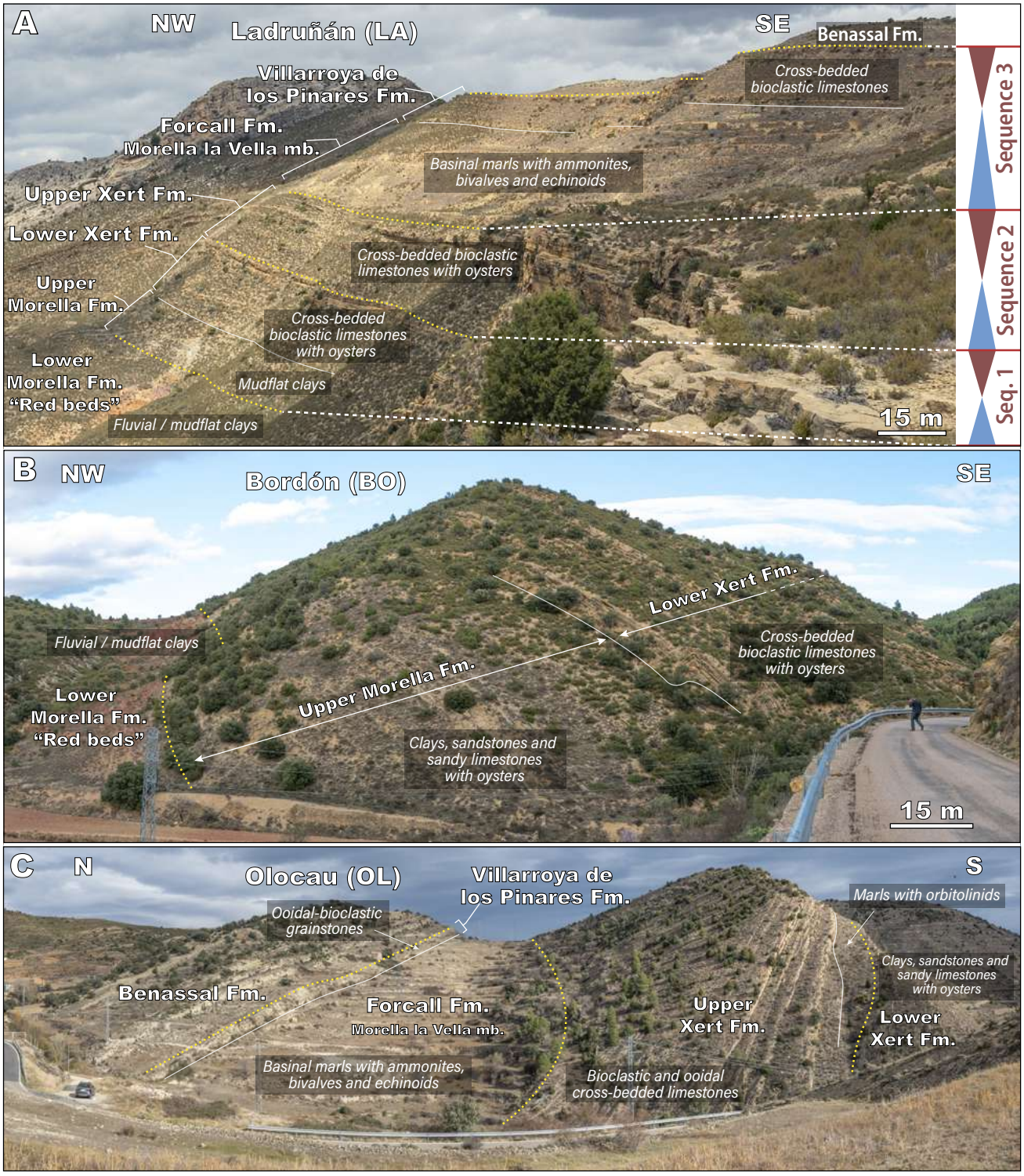

FIGURE 9. Field views showing the distribution of stratigraphic units. A) Ladruñán (LA), B) Luco de Bordón (LB) and C) Olocau (OL). Yellow dotted lines indicate sequence boundaries.

(terebratulids and rhynchonellids), bivalves (including abundant *Plicatula* sp.), orbitolinids and echinoderms. In all the logged localities, marly limestone beds of the lower and middle part of the Forcall Fm. have yielded rich associations of ammonites of the *Deshayesites deshayesi* Zone. Accordingly, in the northern and central area of the Morella subbasin, the Morella la Vella Mb. (upper Forcall Fm.) directly overlies the limestones of the upper Xert Fm. (Fig. 9A).

The Morella la Vella Mb. is overlain by the Villarroya de los Pinares Fm. In JG and AB, this unit is composed of a single cross-bedded bioclastic limestone interval (facies F6), bounded on top by an irregular and ferruginous unconformity surface with evidence of subaerial exposure. In LA and CS, the Villarroya de los Pinares Fm. comprises two grain-supported sandy-bioclastic limestone intervals separated by a mudstone bed of variable thickness, and has an overall thickness ranging from 23 to 30m (Fig. 9A). An ammonite of the upper *Deshayesites deshayesi* Zone (CS, Fig. 7) was collected in the marly interval separating these two bioclastic beds. This upper limestone interval is pervasively dolomitised and iron-stained (facies F6). In the sections of OL-BO and LB the Villarroya de los Pinares Fm. forms a c.5-10m-thick massive to cross-bedded oolitic and bioclastic grainstone bed (facies F7 and F9; Fig. 9C) is topped by an irregular paleokarst. The age of the Villarroya de los Pinares Fm. is well constrained to the upper *Dufrenoyia furcata* Zone in OC (Fig. 4).

Southern Morella subbasin

The new data obtained in CN1-CN2 and MG (Appendix III, Fig. VII) expand the information available from the Morella-Forcall area (*e.g.* Bover-Arnal *et al.*, 2014; Moreno-Bedmar *et al.*, 2010a). In this sector, the fluvial to delta plain red beds of the lower Morella Fm. are topped by a regional transgressive surface located in the middle part of this unit (Bover-Arnal *et al.*, 2016; Gàmez *et al.*, 2003; Salas *et al.*, 1995). Above this surface, there is a gradual transition to the Xert Fm. The thickness of this unit ranges from 45m in CN1 to a maximum thickness around 100m near MO. In MG, the upper part of the Xert Fm. consists of m-thick successions with a lower interval dominated by marls and nodular marly skeletal-rich limestones (facies F2), and an upper interval of cross-bedded, glauconitic, bioclastic packstone-grainstones (facies F6). The Xert Fm. is topped by an encrusted ferruginous surface.

The skeletal marls and limestones of the Cap de Vinyet Mb. and the limestones of the Barra de Morella have variable overall thickness, from 60–90m around MO, to 24m in CN. In MO, the Barra de Morella Mb. corresponds to a c.5m-thick interval of orbitolinid wackestone-packstone with very fine quartz sand (facies F5) and, in CN1, to an 8m-thick alternation of bioclastic marly limestones and bioclastic-ooidal grainstones (facies F7). The upper boundary of this succession is generally a burrowed surface with local encrustation associated with the sharp facies change to the overlying marls of the Morella la Vella Mb. However, in CN1 this discontinuity is a low-relief palaeokarstic surface, which tops a 1m-thick massive oolitic-bioclastic grainstone bed (Fig. 8B).

The thickness of the Morella la Vella Mb. is highly variable, from c.100m around MO, to 22m in CN1CN. Most of the unit consists of open-marine marls (facies F3) with abundant brachiopods, bivalves and ammonites of successive lower Aptian biozones (Moreno-Bedmar *et al.*, 2009, 2010a, b; Fig. 4). In CN1, the lower interval of the Morella la Vella Mb. includes a 3m-thick massive level with abundant coral rubble encrusted by *Lithocodium* (facies F14) developed in the *Deshayesites deshayesi* Zone (Fig. 4).

The lower boundary of the Villarroya de los Pinares Fm. is marked by the abrupt setting of shallow-marine grain-supported carbonates. The thickness of this unit ranges from 10 to 20m across the sector and comprises two unconformity-bounded lithological intervals (Bover-Arnal *et al.*, 2014). The lower interval (3–6m-thick) consists of cross-bedded skeletal grainstones with fragments of bivalves, gastropods, echinoids and bryozoans, as well as intraclasts and peloids (facies F9). The upper interval (c.10m-thick) is dominated by limestones with abundant corals and rudists (facies F15). A well-developed encrusted and bored surface is located either at the boundary between the Villarroya de los Pinares and Benassal formations (*e.g.* MO), or in the upper part of the Villarroya de los Pinares Fm. This unconformity occurs in the upper *Dufrenoyia furcata* Zone (Bover-Arnal *et al.*, 2016).

Western Morella subbasin

During the late Barremian-early Aptian, the western Morella subbasin was under the influence of the Ejulve and Vistabella highs (Fig. 1B). Previous work in this area (Canérot, 1974; Gautier, 1980) described broadly this succession as mostly composed of orbitolinid-rich marlstones and bioclastic limestones, with a relatively reduced thickness ranging from 20 to 60m. Above this succession, the Benassal Fm. consists of well-bedded limestones and marls with abundant *Toucasia* and orbitolinids. The newly logged sections of Barranco de los Degollados (BD) and Cañada de Benatanduz (CB) are representative of the northern and southern domains of this sector, respectively (Fig. VIII, Appendix III).

In BD, the 41m-thick Xert Fm. shows a wide range of facies, from oyster-rich wackestones and fresh-water

carbonates with abundant root traces (Facies F16) to orbitolinid-rich (Facies F4) and cross-bedded ooilitic-peloidal-skeletal limestones (Facies F6, F7, F8, F13). The Xert Fm. is bounded on top by an irregular ferruginous and encrusted surface, which is sharply overlain by a 6m-thick marl interval with abundant orbitolinids, bivalves and brachiopods (facies F3). This interval has been assigned to the upper member of the Forcall Fm. (*i.e.* Morella la Vella Mb.) based on its lithology, fossil content and stratigraphic position below the Villarroya de los Pinares Fm. This latter formation is 16m-thick and includes in its lower part three successive massive coral-*Lithocodium* biostromes (facies F14), with orbitolinid packstone-grainstone interbeds (facies F4). Its upper part consists of an alternation of cross-bedded intraclastic grainstones and peloidal packstones with abundant foraminifera, including orbitolinids (facies F9). This unit is topped by a prominent irregular and iron-stained unconformity, overlain by marls and limestones with orbitolinids and rudists of the lower Benassal Fm.

In the 58m-thick section of CB, the transition between the Morella and Xert formations is marked by successive shallowing upward parasequences topped by sandstones and oyster-rich bioclastic packstone-grainstones (facies F11). Above this interval, most of the Xert Fm. consists of cross-bedded, well-sorted ooidal grainstones (facies F8). The uppermost part of the Xert Fm. includes interbedded mudstones and wackestones with abundant miliolids (facies F13). Above this unit, the 16m-thick Cap de Vinyet Mb. comprises dm-thick levels of oncoidal wackestone-packstones (facies F12), with poorly sorted type 2 and 3 oncoids (Védrine *et al.*, 2007). These facies grade progressively upwards to skeletal-cortoidal (facies F10) grainstones forming a well-cemented 8m-thick interval which has been assigned to the Barra de Morella Mb. The overlying marls of the Morella la Vella Mb. (facies F3) are very reduced in thickness (5m). These marls are sharply overlain by successive coral-*Lithocodium* biostromes (facies F14) of the lower part of the Villarroya de los Pinares Fm. These limestones are locally incised by an erosive surface, infilled by cross-bedded coarse sandstones. These sandstones are in turn overlain by skeletal limestones encrusted by *Lithocodium*, topped by an irregular and iron-rich surface of possible palaeokarstic origin. Above this discontinuity, the succession is dominated by rudist-limestones and marls assigned to the Benassal Fm.

Galve subbasin

The uppermost Barremian-lower Aptian successions of the Galve subbasin heve been previously studied in the outcrops located around AG (Aliaga), MI and VP (Villarroya de Los Pinares) (Bover-Arnal *et al.*, 2009, 2010, 2012, 2015, 2016, 2022, 2024; Embry *et al.*, 2010; Peropadre, 2012; Peropadre *et al.*, 2013; Vennin and Aurell, 2001). In this area there is a gradual transition from the Morella Fm. to the Xert Fm. The lower part of the c.100m-thick Xert Fm. is dominated by thick mudstone intervals, with intercalation of cross-bedded skeletal sandstones and skeletal levels with abundant bivalves, echinoids, orbitolinids and decapod crustaceans (García-Penas *et al.*, 2023). Upwards, the middle part of the unit consists of orbitolinid-rich well-bedded limestones. Ooids and miliolids became abundant in the upper part of the unit, with the local presence of m-thick biostromes of *Chondrodonta* (Bover-Arnal *et al.*, 2010). Towards the western marginal areas of the Galve subbasin, the carbonates of the Xert Fm. pass laterally to cross-bedded sandstones deposited in a shallow water deltaic mouth bar and associated distributaries (Cole *et al.*, 2021). In the marginal area around AG, the Xert Fm. is thinner (c.30m) and is topped by an exposure surface with meteoric to vadose cements (Vennin and Aurell, 2001). However, in the high-subsidence area of MI-VP, the boundary between the Xert Fm. and the overlying Cap de Vinyet Mb. is conformable, or just a minor discontinuity.

The overall thickness of the lower two members of the Forcall Fm. in the subsident domains near MI ranges around 80–90m (Fig. 10A) There, the Cap de Vinyet Mb. comprises burrowed and condensed bioclastic marly limestones with molluscs, orbitolinids and abundant miliolids. The transition from the Cap de Vinyet to the Barra de Morella member is also gradual and marked by the progressive increase of limestone beds rich in orbitolinids with frequent burrowing (mostly *Thalassinoides* and *Planolites*). The overall thickness of these two members is reduced to c.10m around AG, and their identification is not obvious. Vennin and Aurell (2001) attributed this thickness reduction to a transgressive onlap towards the northern marginal areas.

The Morella la Vella Mb. is dominated by marls with successive ammonite-rich levels. In MI, the lower part of the unit includes an up-to-5-m-thick limestone with coral rubble stabilized and encrusted by *Lithocodium aggregatum* which records the OAE1a event (Bover-Arnal *et al.*, 2011). This unit and the overlying Villarroya de los Pinares Fm. form a conformable succession. The last unit is topped by a major unconformity, with deeply incised valleys (50–80m depth) observed near VP (Portolés) and Camarillas (Bover-Arnal *et al.*, 2009, 2022, 2024; Peropadre, 2012). Ammonites of the upper *Dufrenoyia furcata* Zone have been found below and above this unconformity (García-Penas *et al.*, 2023; Moreno-Bedmar *et al.*, 2010a, b).

DISCUSSION

Regional sequence stratigraphy

In this work, the definition and correlation of three unconformity bounded Transgressive-Regressive (TR)

sequences (*sensu* Embry and Johannessen, 1992) in the northwestern Maestrat Basin (referred to here as sequences 1, 2 and 3) assume the age-equivalence of major unconformities identified across the three analysed subbasins (Fig. 11). This assumption is supported by the magnetostratigraphic, ammonite and isotopic data exposed above, combined to the observed vertical and lateral facies evolution. According to the time scale of Gale *et al.* (2020) these three sequences have a duration of c.0.6, 0.8 and 1.3Ma respectively and fit into the range of third-order sequences. They have a transgressive-regressive evolution and are bounded by erosive (frequently palaeokarstic) and/or encrusted (frequently ferruginous and bored) discontinuity surfaces associated with sharp facies changes. Following the nomenclature of Embry and Johannessen (1992) and Catuneanu *et al.* (2011), we have differentiated a lower Transgressive Systems Tract (TST) and an upper Regressive Systems Tract (RST). These two hemicycles are separated by a maximum flooding surface (mfs.) or zone (mfz.). Although the definition of TR sequences depends solely on changes in depositional trends and the recognition of maximum regressive surfaces, we make occasional references to stratal stacking patterns and geometries where relevant. The main features and time calibration of these sequences are summarized below.

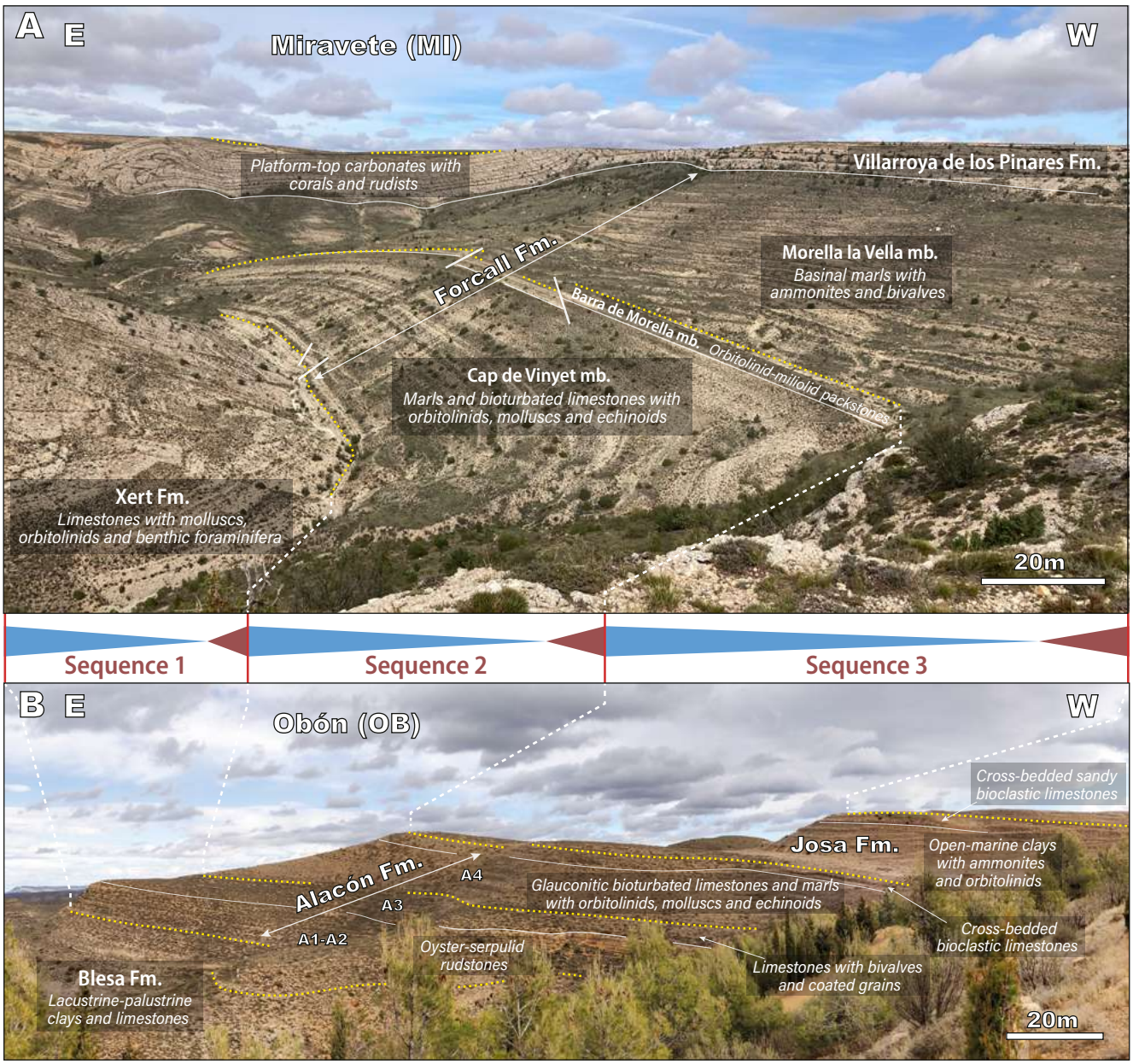

FIGURE 10. Comparison of sequences 1-3 in the Galve and Oliete subbasins. Yellow dashed lines indicate major unconformities. Yellow dotted lines indicate sequence boundaries.

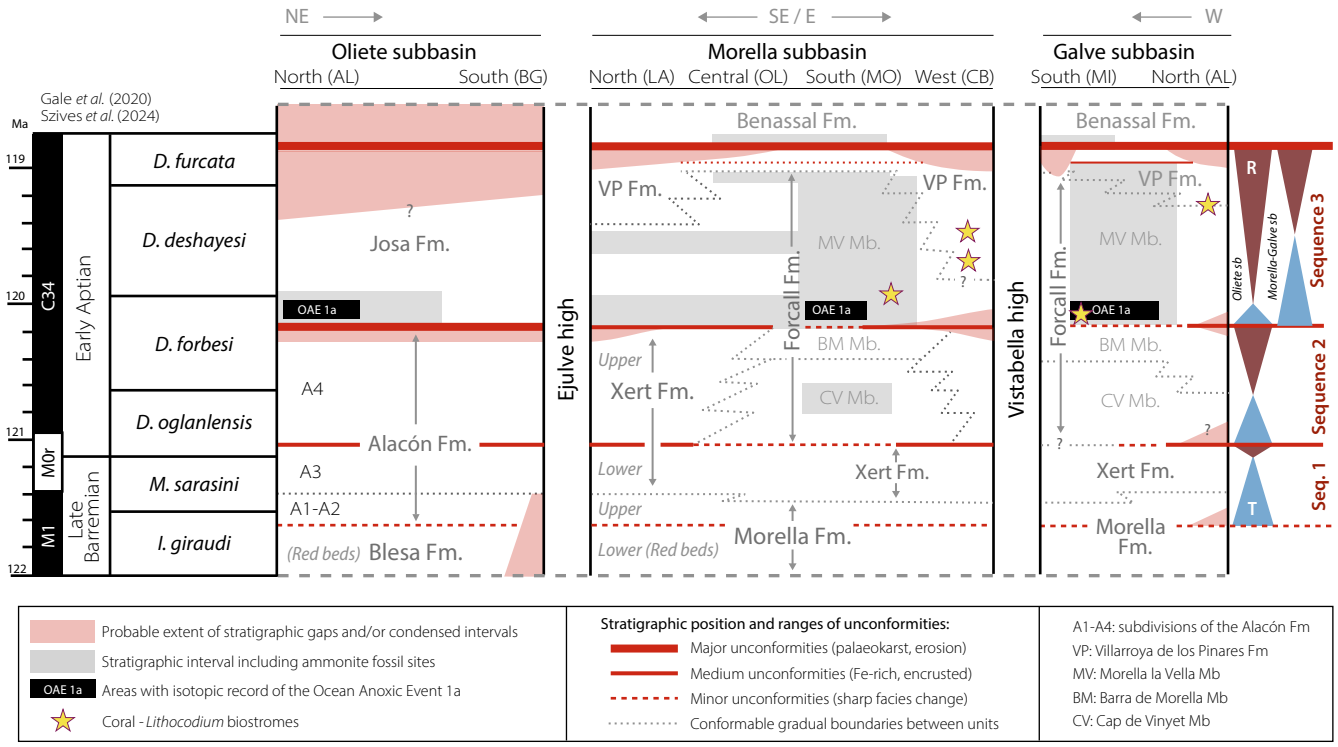

FIGURE 11. Chronostratigraphic chart of the studied lithostratigraphic units and TR sequences along with their age calibration in the Oliete, Morella and Galve subbasins. A1-4 represent the higher order sequences interpreted by García-Penas *et al.* (2022) in the Alacón Fm. In the Morella and Galve subbasin, the Morella and Xert formations are divided into two informal lower and upper subunits.

Sequence 1

This sequence was mostly developed during the latest Barremian (Fig. 11), and includes the lower Alacón Fm. (Oliete subbasin), the upper Morella-lower Xert formations (norther-central Morella subbasin), and the upper Morella-Xert formations (southern Morella and Galve subbasins).

In the Morella and Galve subbasins, the lower boundary of Sequence 1 is located between the lower (continental red beds) and upper part (coastal grey mudstones and sandstones) of the Morella Fm. (see lower and upper Morella in Fig. 11). This boundary was placed in the middle part of the *Imerites giraudi* Zone based on ammonite and strontium-isotope data (Bover-Arnal *et al.*, 2016). The equivalent boundary in the Oliete subbasin is found between the Blesa and Alacón formations (Aurell *et al.*, 2018; García-Penas *et al.*, 2022), in the upper part of magnetozone M1 (Figs. 10B; 11). These data support the proposed time-equivalence of the transgressive event that marks the lower boundary of Sequence 1 across the Oliete, Morella and Galve subbasins.

In the Oliete subbasin, Sequence 1 consists of a long TST involving the progressive appearance of shallow-marine limestones across the studied domains, locally forming onlap geometries over the Jurassic substrate (Fig. 2C). The mfs. has only been reliably identified in this subbasin, where it is associated with massive accumulations of glauconite (García-Penas *et al.*, 2022). Above the mfs., a short-lived RST spans the middle part of the Alacón Fm. (Oliete subbasin), the upper part of the lower Xert Fm. (northern-central Morella subbasin), or the upper levels of the Xert Fm. (depocentral areas of the Morella and Galve subbasins).

The expression of the upper sequence boundary varies across the study area. In the Oliete subbasin, and in marginal areas of the Morella subbasin, it corresponds to a well-developed burrowed and Fe-encrusted unconformity (boundary between sequences A3 and A4, Fig. 10B). In the depocentral areas of the Galve and Morella subbasins, however, the boundary between the Xert and Forcall formations is conformable, or just a minor unconformity. The magnetostratigraphic data reported here indicates that this boundary is located in the upper part of polarity chron M0r, close to the Barremian-Aptian stage boundary (Fig. 11).

Sequence 2

This sequence is earliest Aptian in age (Fig. 11) and includes the upper Alacón Fm. (Oliete subbasin), the upper Xert Fm. (northern-central Morella subbasin), and the

Cap de Vinyet and Barra de Morella members (southern Morella and Galve subbasins).

The TST consists of open marine facies in depocentral areas, with local onlap geometries described in marginal areas of the Galve subbasin (Aurell and Vennin, 2001). In the open-marine domain of the southern Morella subbasin, the mfz. is marked by the local presence of ammonites around the boundary between the *Deshayesites oglanlensis* and *Deshayesites forbesi* zones around the middle part of the Cap de Vinyet Mb. In the Oliete subbasin, the mfz. is located in the upper part of the Alacón Fm. (*i.e.* middle part of sequence A4, Fig. 10B), in the lower part of magnetozone C34. These data support the time-equivalence of the mfz. of Sequence 2 in the Oliete, Morella and Galve subbasins (Fig. 11). The RST is composed of cross-bedded bioclastic grainstones in the Oliete subbasin (*i.e.* upper part of A4 sequence) and in marginal areas of the Morella subbasin (*i.e.* upper part of the upper Xert Fm.). These bioclastic regressive facies grade laterally (in the southern Morella and Galve subbasins) into orbitolinid and ooid-rich grain-supported limestones of the Barra de Morella Mb. (Fig. 10A).

In the Oliete subbasin and in marginal areas of the Morella subbasin, the upper sequence boundary is a paleokarst topping the Alacón (Fig. 8A) and Xert formations. This boundary is associated with a stratigraphic gap of uncertain duration spanning part of the *Deshayesites oglanlensis* and *Deshayesites forbesi* zones (Fig. 11). However, in the depocentral areas of the Morella and Galve subbasins, this surface changes into a minor unconformity or a correlative conformity topping the Barra de Morella Mb. Locally, however, a paleokarst tops this unit in the southern Morella sb. (Fig. 8B).

Sequence 3

This upper-lower Aptian sequence includes the Josa, upper Forcall (Morella la Vella Mb.) and Villarroya de los Pinares formations (Fig. 11). In the depocentral areas of the three studied subbasins, the onset of the sequence is generally marked by the presence of a 10–20m thick marly interval which records the OAE 1a, spanning the late *Deshayesites forbesi* Zone (*e.g.* Moreno-Bedmar *et al.*, 2010a). However, we have not found any isotopic evidence of this event in the northern marginal areas of the Morella subbasin (Fig. 7).

In the Oliete subbasin, above the OAE 1a equivalent interval, the Josa Fm. shows an upwards regressive trend characterised by a progressive increase in sandstone tempestites. However, in the Morella and Galve subbasins, open-marine conditions persist above the record of the OAE1a, as indicated by the almost continuous ammonite record in the Morella la Vella Mb. In these areas, the mfz. is located around the middle-upper part of the *Deshayesites deshayesi* Zone, owing to the widespread occurrence of thick intervals of dark-blue marls bearing abundant deshayesitid ammonites (Moreno-Bedmar *et al.*, 2010a, b; Peropadre, 2012), not only in the depocentral areas of the Galve and Morella subbasins, but also in the marginal areas (Fig. 4). The time offset of the mfz. between the Oliete subbasin and the Galve and Morella subbasins (Fig. 11) can be attributed to the intense terrigenous input in the Oliete subbasin, which may have offset the accommodation generated by sea-level rise.

Coral biostromes encrusted by *Lithocodium* are common in the Morella and Galve subbasins in different time intervals (Fig. 11). In the Galve subbasin (MI) a distinct biostrome occurs in the upper *Deshayesites forbesi* Zone (Bover-Arnal *et al.*, 2011; Moreno-Bedmar *et al.*, 2009). In the southeastern Morella subbasin (CN1), a biostrome located in the lower Morella la Vella Mb. occurs in the *Deshayesites deshayesi* Zone. In the western Morella subbasin successive biostromes in the lower Villarroya de los Pinares Fm. likely occur within the *Deshayesites deshayesi* Zone, around the mfz.

The upper sequence boundary is the major unconformity with evidence of subaerial exposure found on top of the Villarroya de los Pinares Fm. (Morella and Galve subbasins) and on top of the Josa Fm. (Oliete subbasin). The age of this unconformity in the depocentral areas of the Galve and Morella subbasins is well constrained to the upper *Dufrenoyia furcata* Zone (Fig. 11). In the northern Morella subbasin, the youngest ammonites recorded in Sequence 3 belong to the upper *Deshayesites deshayesi* Zone, and the gap associated to the unconformity is assumed to span most of the *Dufrenoyia furcata* Zone (Fig. 11). In the Oliete subbasin, there is no record of ammonites of the *Deshayesites deshayesi* and *Dufrenoyia furcata* zones, and the gap is assumed to be more extensive (Fig. 11). The truncation surface associated with the unconformity involved a sea-level fall with an amplitude of around 50–80m in the Galve subbasin (Bover-Arnal *et al.*, 2009, 2022, 2024; Peropadre, 2012; Peropadre *et al.*, 2013). Low-relief erosive incisions on top of the Villarroya de los Pinares and Josa formations are also observed in western marginal areas of the Morella subbasin and in the Oliete subbasin. However, in most of the study area this upper unconformity is a flat low-relief erosive surface.

A higher-order unconformity (developed also in the *Dufrenoyia furcata* Zone) is recorded in the Galve and southern Morella subbasins in the lower or middle part of the Villarroya de los Pinares Fm., in the upper part of Sequence 3 (Fig. 11). East of MI, this subordinate unconformity overlies forced-regressive deposits with

offlap geometries related to a relative sea-level fall (see FRST of Sequence S2 in Vennin and Aurell, 2001). Forced-regressive deposits were also documented west of MI (*i.e.* FRWST of Depositional Sequence A, Mingachas outcrop; Bover-Arnal *et al.*, 2009, 2022). In the southern Morella and Galve subbasins, this minor order discontinuity is overlain by rudist-coral carbonate platforms developed during the relative sea-level lowstand of the upper RST of Sequence 2 (upper Villarroya de los Pinares Fm.; Fig. 11).

Sedimentary evolution

This section aims to reconstruct the sedimentary evolution of the northeastern Maestrat Basin during the latest Barremian-early Aptian. The proximal-distal facies transects and facies distribution maps shown in Figure 12 are based on the correlation of lithostratigraphic units and TR sequences justified in previous sections. The lower part of Sequence 1 is not well exposed across all studied areas, and its vertical and lateral facies distribution cannot be reconstructed in detail. Above this sequence, the facies evolution is shown in four successive stages, around the mfz. of Sequence 2 and Sequence 3 (Fig. 12C, D), and during the RST of Sequence 3 (Fig. 12E, F). In these maps, data of the adjacent Las Parras and western Galve subbasins is mostly based on Clariana (1999), Vennin and Aurell (2001), Bover-Arnal *et al.* (2010) and Peropadre (2012).

Sequence 1

In the more marginal areas of the Oliete subbasin, the TST of Sequence 1 is characterised by bioclastic calcareous and terrigenous facies with mollusks and ostracods, which grade upwards into skeletal facies with more diverse benthic associations (Appendix III, Fig. III). These facies were sedimented in intertidal to shallow subtidal environments of a shallow bay influenced by frequent salinity oscillations (García-Penas *et al.*, 2022).

In the more open-marine domains of the Morella and Galve subbasins, the age-equivalent units record a gradual transition from coastal-deltaic terrigenous dominated environments (upper Morella Fm.) to shallow marine carbonate platform settings (Xert Fm.; Bover-Arnal *et al.*, 2010; Embry *et al.*, 2010; Salas *et al.*, 1995).

In the Oliete subbasin, a stabilization of normal marine conditions can be interpreted in the upper part of the sequence based on an increase in diversity of the faunal associations (García-Penas *et al.*, 2022). Basinwards, in the more open-marine areas of the Galve and Morella subbasins, the platform flooding involved the progressive setting of orbitolinid-rich shallow-marine environments (*e.g.* Bover-Arnal *et al.*, 2010; Peropadre, 2012; Vennin and Aurell, 2001).

Sequence 2

In the Oliete subbasin, Sequence 2 is characterised by clays and mud-supported limestones containing gryphaeid oysters, other bivalves, gastropods, echinoids and orbitolinids. These materials represent a low-energy lagoonal environment, subject to environmental stress related to freshwater influxes and reduced marine circulation (García-Penas *et al.*, 2022). Water depth diminished towards the relatively uplifted eastern margin of the subbasin (Ejulve High, Fig. 12C). There, Sequence 2 is entirely composed of moderately sorted, bioclastic, coarse-grained packstones and grainstones. Locally, these deposits are pervasively dolomitised (Appendix II, Fig. IV), which has been attributed to episodic subaerial exposure (García-Penas *et al.*, 2022). We interpret these facies as shoal and backshoal deposits (*e.g.* Bádenas and Aurell, 2010), forming part of an extensive shoal system which extended over the Ejulve High and the northern and central Morella subbasin, shielding the Oliete subbasin from direct marine influence (Fig. 12C).

In the central Morella subbasin (BO, OL), bioclastic facies co-occur with well-sorted peloidal and oolitic grainstones (Appendix III, Fig. VI). Lack of evidence of subaerial exposure, small grain sizes and good sorting suggest that these facies were deposited in deeper environments than the purely bioclastic deposits which predominate in the north. We interpret that these facies represent shoal-foreshoal environments, developed around the inner-to-mid-ramp transition, where the fair weather and storm waves interact with the substrate intensely (Bádenas and Aurell, 2010).

In the distal sections of the southern Morella subbasin (MG, CN1), the TST and most of the RST are dominated by marls and marly limestones with abundant open-marine fauna, including bivalves, echinoids, colonial corals and scarce ammonites. These facies are interpreted as low-energy proximal-offshore deposits (Fig. 12C). Intercalations of cross-bedded skeletal limestones (around Forcall, Fig. 12B) are interpreted as storm-influenced shoals with resedimented skeletal components.

In MG, the uppermost part of the RST comprises orbitolinid sandstones (Fig. 12B) which are interpreted to represent a low-energy, possibly nearshore, environment influenced by siliciclastic inputs, developed during the latter stages of marine regression. Equivalent levels in CN1 and MO are characterised by the progressive intercalation of skeletal grainstones with ooids, bioclasts with micritic coatings, and intraclasts. The onset of these high-energy deposits reflects the progradation of shallow high-energy shoal environments from the Vistabella High and the northeastern margin of the Maestrat Basin (Fig. 12B).

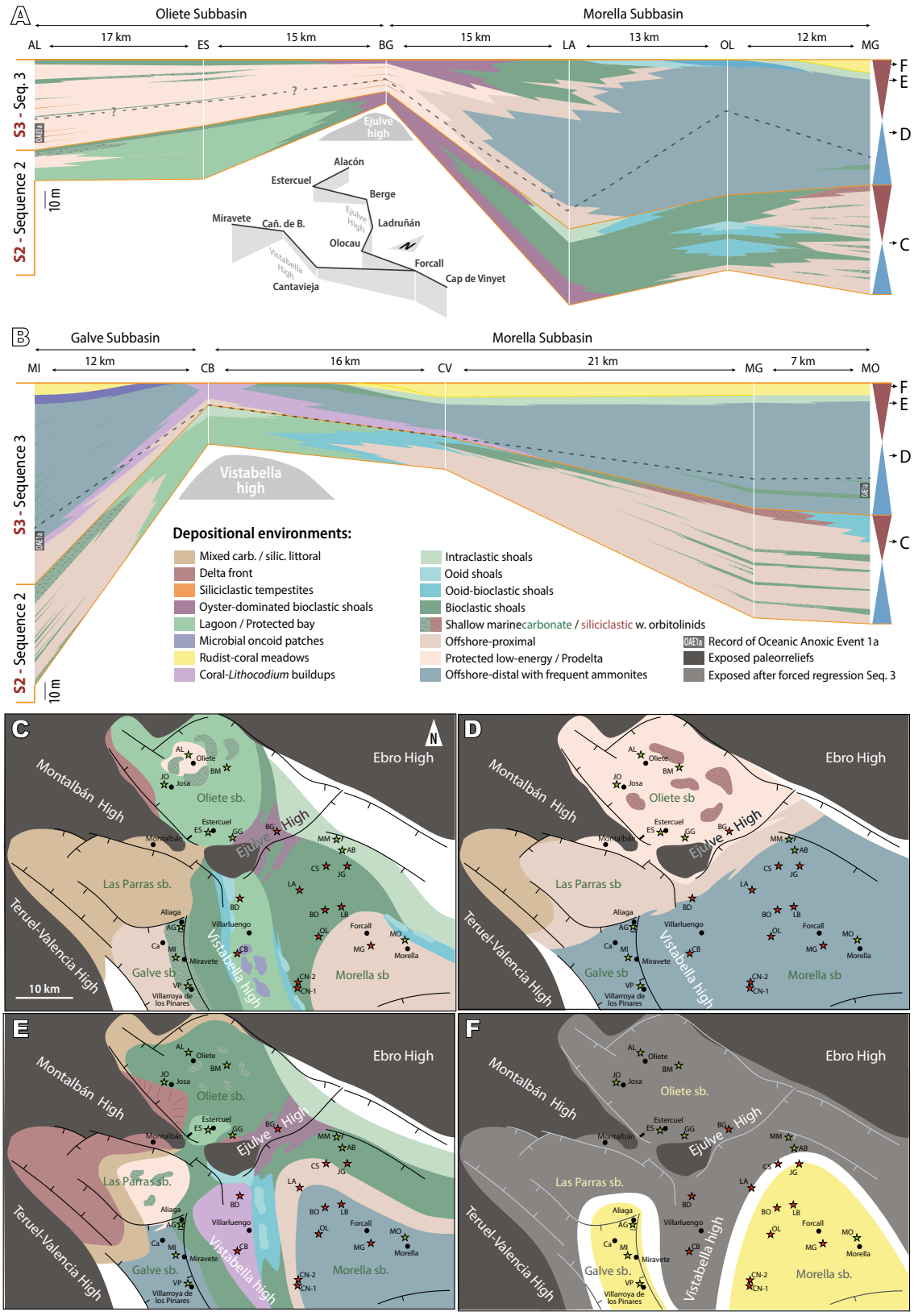

FIGURE 12. A, B) Cross sections showing the distribution of palaeoenvironments in the lower Aptian depositional sequences 2 and 3 across the studied subbasins. Dashed line indicates the boundary between the *Deshayesites forbesi* and *Deshayesites deshayesi* zones. The idealized palaeoenvironment distribution is shown in successive non-palinspastic maps C) for the middle part of Sequence 2 and D) for the lower, E) middle and F) uppermost part of Sequence 3.

In the northern part of the Vistabella High (BD), Sequence 2 is quite homogeneous, comprising mud-supported limestones with abundant miliolids and root traces. In the southern part (CB), these same facies also present intercalations of bioclastic wackestones with microbial oncoids. The depositional environment of these facies is interpreted as a relatively deep lagoon (Fig. 12B, C), influenced by episodic storm-induced waves (Flügel, 2010; Védrine *et al.*, 2007). Based on the occurrence of ooidal facies in CN1, we interpret that the lagoon was probably linked to the open-marine areas of the central Morella subbasin through shoals developed on the western margin of the subbasin (Fig. 12C).

In the southern Galve subbasin, the TST comprises orbitolinid-rich wackestone-packstones and marls sedimented in proximal-offshore environments (Bover-Arnal *et al.*, 2010; Peropadre, 2012). The northern marginal areas of the subbasin are characterised by mud-supported orbitolinid limestones with abundant terrigenous inputs, suggesting deposition in very proximal lagoonal environments (Peropadre, 2012). The RST is homogeneous across the Galve subbasin, comprising shallow and marginal-marine environments dominated by orbitolinids and mollusks (Bover-Arnal *et al.*, 2010; Embry *et al.*, 2010).

In the transitional areas between the Las Parras and Galve subbasins, the lithology of Sequence 2 is quite homogeneous, being characterised by skeletal mudstones with sandy limestone intercalations which represent quiet and very shallow marine environments (Clariana, 1999; Peropadre, 2012).

Sequence 3

In the Oliete subbasin, the short TST, and most of the RST of Sequence 3 correspond to mudstones deposited in a prodelta environment. Frequent intercalations of sandstones with hummocky cross-lamination, attributed to intense episodic riverine inputs along the western and northern margins of the subbasin (García-Penas *et al.*, 2024). The progradation of a deltaic system during late regression led to the setting of mudflats in the northwestern coastal areas (García-Penas *et al.*, 2024), and of a very shallow-marine delta front along the western margin of the subbasin (Fig. 12E). This latter setting was inhabited by diverse mollusc communities with scarce stenohaline fauna (ammonites, bryozoans, corals). These faunal assemblages reflect fluctuations of environmental conditions (salinity, substrate oxygenation) derived from restricted marine circulation (García-Penas *et al.*, 2024). Marine circulation was hampered by an extensive shoal system developed over the Ejulve High (Fig. 12E), characterised by shallow-marine bioclastic subtidal dunes. Northwards, these facies grade laterally into intraclastic grainstones, which are interpreted as high-energy marginal-marine deposits.

In most of the Morella and Galve subbasins, the TST is characterised by basinal marls with local intercalations of coral-*Lithocodium* biostromes (Fig. 12B). The stratigraphic position of these biostromes and the abundance of disarticulated coral rubble suggest a depositional setting close to the platform margin or upper slope, where colonial corals were most abundant (Bover-Arnal *et al.*, 2012; Michel *et al.*, 2023). The massive tabular morphology of these bodies is also typical of *Lithocodium* buildups developed under moderate to high energy conditions in platform margins (Rameil *et al.*, 2010). The proliferation of *Lithocodium*-rich facies across the Tethys during the Aptian has been related to increased nutrient levels caused by marine transgression over coastal lowlands, and to increased water alkalinity fostering the activity of carbonate producers (Immenhauser *et al.*, 2005).

In the Morella and Galve subbasins, the RST is represented by the shallow-marine carbonates of the Villarroya de los Pinares Fm. Relative sea-level fall at the end of this sequence led to the progressive subaerial exposure of vast areas of the Oliete, Galve and Morella subbasins (Fig. 12F), producing a karstified and iron-stained subaerial unconformity recognisable across the study area. In the northern marginal areas of the Morella subbasin (see the interval between BG and OL in Fig. 12A), the Villarroya de los Pinares Fm. comprises two offlapping bioclastic grainstone wedges of different age (upper *Deshayesites deshayesi* and *Dufrenoyia furcata* zones respectively), that pass basinwards into open-marine marls. Ooidal grainstones of the Villarroya de los Pinares Fm. in BO-OL are also interpreted here as a younger forced-regressive wedge (Fig. 12A). Further south in the Morella subbasin, these regressive wedges consist of cross-bedded skeletal-intraclastic grainstones. Several localities in the Galve subbasin also preserve forced-regressive wedges dominated by bioclastic facies and coral-rudist reefs (Bover-Arnal *et al.*, 2010, 2016, 2022, 2024; Vennin and Aurell, 2001). The late RST comprises coral-rudist platforms in the southern domains of the Galve and Morella subbasins (see Fig. 12F). A dm-thick rudist floatstone bed topping the bioclastic deposits of the Villarroya de los Pinares in JG represents the northernmost extent of these platforms. These platforms were eventually exposed subaerially, resulting in the development of a paleokarst on top of the Villarroya de los Pinares Fm. (*e.g.* Bover-Arnal *et al.*, 2022, 2024).

Chronostratigraphy and regional correlation

The lithostratigraphic and sequence stratigraphical framework proposed in this work for the Morella and Oliete

subbasins improve the chronostratigraphic resolution of the uppermost Barremian-lower Aptian succession of the NW Maestrat Basin. The precise identification of the M0r magnetozone in the middle part of the Alacón Fm. is especially relevant, as there is almost no palaeomagnetic data from the Lower Cretaceous of the Maestrat Basin due to the extensive remagnetisation of the pre-Albian succession (*e.g.* Juárez *et al.*, 1998). In this section we discuss the implications of the obtained results in light of previous interpretations (Fig. 13).

The age and lateral correlation of the Alacón Fm. has been debated over the last years. Canérot *et al.* (1982) defined this unit and proposed a late Barremian-earliest Aptian age based on the presence in its upper part of *Palorbitolina lenticularis*, which was considered as a biostratigraphic marker for the lower Aptian of Iberia. Since then, the regional stratigraphic range of this taxon has been extended into the upper Barremian (*e.g.* Bover-Arnal *et al.*, 2016). The upper part of this formation was regarded as lateral equivalent of the Morella and Xert formations. Salas (1987), Soria (1997) and Salas *et al.* (2001) assigned the same age range, but considered the Alacón Fm. as a lateral equivalent of the Artoles Fm.

The correlation of the Oliete and Morella subbasins proposed in Moreno-Bedmar *et al.* (2010a, b) shows the Alacón Fm. as lateral equivalent of the Artoles, Morella and Xert formations (Fig. 13A). These authors regarded the Morella and Xert formations as earliest Aptian in age. In the Oliete subbasin, a large stratigraphic gap was proposed between the Alacón and Forcall formations. This gap would be coeval to the sedimentation of the Cap de Vinyet and Barra de Morella members in the more open marine areas of the Morella subbasin. In a regional stratigraphic synthesis including data from the Morella subbasin, Bover-Arnal *et al.* (2016) proposed a latest Barremian age for the Morella and Xert formations (Fig. 13B). The boundary between these two units was placed in the lowermost part of the *Martelites sarasini* Zone. The correlation proposals by Aurell *et al.* (2018) and García-Penas *et al.* (2023) took into account these interpretations (Fig. 13C). However, the authors considered the upper part of the Blesa Fm. as equivalent in age to the Morella Fm., whereas the Alacón Fm. was considered to span the same age range as the Xert Fm. and the lower member of the Forcall Fm. (*i.e.* Cap de Vinyet Mb.). The amplitude of the stratigraphic gap between the Alacón and the newly defined Josa Fm. (see García-Penas *et al.*, 2024) was reduced compared to the previous proposal by Moreno-Bedmar *et al.* (2010a, b). This gap was regarded as coeval with the regressive event indicated by the Barra de Morella Mb. in the southern Morella subbasin. Above this unit, the age of the upper member of the Forcall Fm. (*i.e.* Morella la Vella Mb.) and the overlying Villarroya de los Pinares Fm. was well defined in the Morella subbasin due to the abundance of ammonites (*e.g.* Bover-Arnal *et al.*, 2016; Moreno-Bedmar *et al.*, 2010a).

The correlation proposed in this work (Fig. 13D) indicates that the lower boundary of the Alacón Fm. is of the same age as the transgressive surface found in the middle part of the Morella Fm. (*i.e.* boundary between the upper and lower Morella Fm. in Fig. 13). This boundary corresponds to the lower boundary of TR Sequence II of Bover-Arnal *et al.* (2016). The data and interpretations reported here are coherent with the latest Barremian age proposed by these authors for this sequence boundary, and for the boundary between the Morella and Xert formations. The proposed correlation also implies that the Barremian-Aptian stage boundary is located around the boundary between the Xert Fm. and the Cap de Vinyet Mb. (Fig. 12).

The new stratigraphic and sedimentological data obtained in the northern and central areas of the Morella subbasin were also of paramount importance to understand the lateral equivalence between the Alacón Fm., the Xert Fm., and the lower two members of the Forcall Fm. (Fig. 13D). In particular, the lithological and facies evolution reconstructed in the area linking the Oliete subbasin and the more open-marine Morella subbasin (see Sequence 2 in Fig. 12A,B) supports the age equivalence between the upper part of the Alacón Fm. (or sequence A4 of García-Penas *et al.*, 2022) and the succession comprising the upper Xert Fm., and the Cap de Vinyet and Barra de Morella members. The extent of the gap associated with the unconformity found on top of the Alacón Fm. is uncertain. However, the reconstructed lateral and vertical configuration of the RST of Sequence 2 suggest that the amplitude of this gap was overestimated in previous work.

CONCLUDING REMARKS

New stratigraphic and sedimentological data from the marginal and central areas of the Morella subbasin (Maestrat Basin) refine the correlation of the uppermost Barremian-lower Aptian units previously studied in the Oliete subbasin, and in the depocentral areas of the Galve and Morella subbasins. In the Oliete subbasin, the studied succession corresponds to the Alacón and Josa formations. In the Galve and Morella subbasins, the equivalent units include the Xert, Forcall and Villarroya de los Pinares formations. These units are arranged into three third-order sequences bounded by unconformities, which can be traced across all the analysed subbasins:

Sequence 1 includes the lower part of the Alacón and Xert formations in the Oliete and in the northern-central

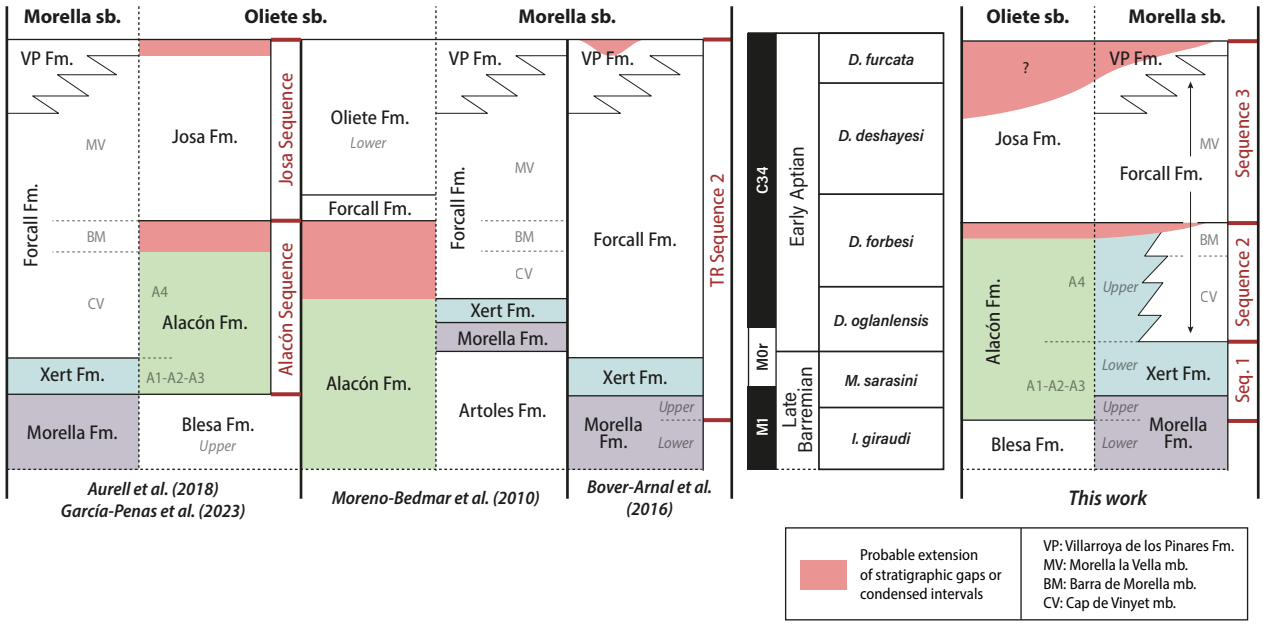

FIGURE 13. Correlation of stratigraphic units and sequences proposed in previous work (A-B-C), compared to this study (D). A1-4 represent the higher order sequences interpreted by García-Penas *et al.* (2022) in the Alacón Fm. In the Morella subbasin, the Morella and Xert formations are divided into two informal lower and upper subunits.

Morella subbasin respectively, and the whole Xert Fm. in the Galve and southern Morella subbasins.

Sequence 2 corresponds to the marls and shallow-marine limestones of the upper part of the Alacón and Xert formations (Oliete and northern-central Morella subbasins), which pass to the lower (Cap de Vinyet) and middle (Barra de Morella) members of the Forcall Fm. in the Galve and southern Morella subbasins.

Sequence 3 comprises the Josa Fm. (Oliete subbasin) and its basinwards counterparts, the open-marine marls of the upper Forcall Fm. (Morella la Vella Mb.), and the shallow-marine limestones of the Villarroya de los Pinares Fm.

The proposed sequence stratigraphic framework allows the reconstruction of the overall facies distribution and palaeogeography in successive depositional stages. As a result, this work documents for the first time the sedimentary evolution and facies transition between the northern, marginal protected areas of the Oliete subbasin, to the southern, open-marine areas of the Morella subbasin.

Magnetostratigraphic analysis in the Oliete subbasin resulted in the identification of the M0r magnetozone in the middle part of the Alacón Fm. The lower boundary of this magnetozone is found in the middle part of Sequence 1, while its upper boundary is located in the lowermost levels of Sequence 2. These results support the basinwide correlation of the depositional sequences identified in this work, also providing further chronostratigraphic constraints. In particular:

i) The lower boundary of Sequence 1 is a widespread transgressive surface involving a sharp transition from the red continental beds of the lower Morella/upper Blesa formations to the grey sandstones and restricted marine limestones of the upper Morella/lower Alacón formations. The reported data suggest that transgression across the NW Maestrat Basin occurred in an isochronous manner during the mid-late Barremian (upper *Imerites giraudi* Zone), as proposed in previous studies.

ii) Magnetostratigraphy in the Oliete subbasin suggest that the Barremian-Aptian stage boundary is located near the boundary between sequences 1 and 2. According to the proposed correlation, this stage boundary is located around the lithostratigraphic boundary between the Xert and Forcall (Cap de Vinyet Mb.) formations.

iii) The boundary between sequences 2 and 3 is a major, early Aptian (intra *Deshayesites forbesi* Zone), unconformity found either on top of the Alacón Fm. (in the Oliete subbasin), or on top of the Xert Fm. (in marginal areas of the Galve and Morella subbasin). This unconformity is equivalent to a minor unconformity which tops the Barra de Morella Mb. in the more open-marine areas of the southern Morella and Galve subbasins.

iv) Intense detrital inputs in the Oliete subbasin explain the observed temporal offset of the TST of Sequence 3. In the Oliete subbasin, it comprises the upper *Deshayesites forbesi* Zone, whereas in the Galve and Morella subbasins the TST spans also most of the *Deshayesites deshayesi* Zone.

v) The upper boundary of Sequence 3 is a major, latest early Aptian (intra-*Dufrenoyia furcata* Zone), unconformity. This unconformity, which was attributed in previous studies to a high-amplitude eustatic sea-level fall, has been further documented here as a widespread palaeokarstic and erosive surface developed on top of the Josa and Villarroya de los Pinares formations, indicating the subaerial exposure of most of the study area. Forced-regressive wedges have been further documented here in the marginal areas of the Morella subbasin.

ACKNOWLEDGMENTS

The authors deeply appreciate the learning and friendship shared by our colleague Ramon Salas over the last decades. Therefore, we are proud to contribute to this special volume dedicated to Ramon, and we want to express our gratitude to the editorial board of Geologica Acta for giving us this opportunity. Special thanks are also due to Telm Bover-Arnal, who actively contributed to the exchange of ideas and data during all stages of this research. The editorial work done by Joan Guimerà and two anonymous reviewers is also deeply acknowledged. This paper was funded by projects PID2021-122612OBI00, PID2019-108753GB-C21 and Group E18 (Aragosaurus: Recursos Geológicos y Palaeoambientes) subsidized by the Ministerio de Ciencia e Innovación, the European Regional Development Fund and the Government of Aragón, as well as the project IBERINSULA (PID2020-113912GB-I00), funded by MCIN/AEI/10.13039/501100011033 and the European Regional Development Fund (ERDF). Álvaro García-Penas has a predoctoral contract (contract code PRE2018-084468) co-financed by the Spanish Government and the European Social Fund (ESF). The authors would also like to acknowledge the support of the Servicio General de Apoyo a la Investigación-SAI, Universidad de Zaragoza, and thank Diego Rubio and José Martín for donating two ammonites from the Oliete Subbasin.

DATA AVAILABILITY

Raw paleomagnetic data are available in Calvín *et al.* (2024).

REFERENCES

Aurell, M., Soria, A.R., Bádenas, B., Liesa, C.L., Canudo, J.I., Gasca, J.M., Moreno-Azanza, M., Medrano-Aguado, E., Meléndez, A., 2018. Barremian synrift sedimentation in the Oliete subbasin (Iberian Basin, Spain): palaeogeographical evolution and distribution of vertebrate remains. Journal of Iberian Geology, 44, 285-308.

Aurell, M., Bádenas, B., Canudo, J.I., Castanera, D., García-Penas, A., Gasca, J.M., Val, J., 2019a. Kimmeridgian-Berriasian stratigraphy and sedimentary evolution of the central Iberian Rift System (NE Spain). Cretaceous Research, 103, 104153.

Aurell, M., Fregenal-Martínez, M., Bádenas, B., Muñoz-García, M.B., Élez, J., Meléndez, N., de Santisteban, C., 2019b. Middle Jurassic–Early Cretaceous tectono-sedimentary evolution of the southwestern Iberian Basin (central Spain): major palaeogeographical changes in the geotectonic framework of the Western Tethys. Earth-Science Reviews, 199, 102983.

Bádenas, B., Aurell, M., 2010. Facies models of a shallow-water carbonate ramp based on distribution of non-skeletal grains (Kimmeridgian, Spain). Facies, 56, 89-110.

Baraboshkin, E.J., 2005. Boreal-Tethyan correlation of Lower Cretaceous ammonite scales. Moscow University, Geology Bulletin, 59 (2004, 6), 9-20.

Baudouin, C., Delanoy, G., Moreno-Bedmar, J.A., Pictet, A., Vermeulen, J., Conte, G., Gonnet, R., Boselli, P., Boselli, M., 2016. Revision of the Early Cretaceous genera *Heminautilus* SPATH, 1927, and *Josanautilus* Martínez & Grauges, 2006 (Nautilida, Cenoceratidae). Carnets de Géologie [Notebooks on Geology], 16(5), 61-212.

Bogdanova, T.N., 1983. *Deshayesites tuarkyricus* Zone-the lowermost zone of the Aptian in Turkmenistan (In Russian). Ezhegodnik Vsesojuznogo Paleontologicheskogo Obshchestva (Akademiya Nauk SSSR), 26, 128-147.

Bover-Arnal, T., Salas, R., 2019. Geology of the 'Sénia stone' from Ulldecona, Catalonia (Aptian, Maestrat Basin, Iberian Chain) and its implications for regional stratigraphy. Cretaceous Research, 96, 38-58.

Bover-Arnal, T., Salas, R., Moreno-Bedmar, J.A., Bitzer, K., 2009. Sequence stratigraphy and architecture of a late Early–Middle Aptian carbonate platform succession from the western Maestrat Basin (Iberian Chain, Spain). Sedimentary Geology, 219, 280-301.

Bover-Arnal, T., Moreno-Bedmar, J.A., Salas, R., Skelton, P.W., Bitzer, K., Gili, E., 2010. Sedimentary evolution of an Aptian syn-rift carbonate system (Maestrat Basin, E Spain): effects of accommodation and environmental change. Geologica Acta, 8(3), 249-280.

Bover-Arnal, T., Salas, R., Martín-Closas, C., Schlagintweit, F., Moreno-Bedmar, J.A., 2011. Expression of an oceanic anoxic event in a neritic setting: lower Aptian coral rubble deposits from the western Maestrat Basin (Iberian Chain, Spain). Palaios, 26, 18-32.

Bover-Arnal, T., Löser, H., Moreno-Bedmar, J.A., Salas, R., Strasser, A., 2012. Corals on the slope (Aptian, Maestrat Basin, Spain). Cretaceous Research, 37, 43-64.

Bover-Arnal, T., Salas, R., Guimerà, J., Moreno-Bedmar, J.A., 2014. Deep incision on an Aptian carbonate succession indicates

major sea-level fall in the Cretaceous. Sedimentology, 61, 1558-1593.

Bover-Arnal, T., Pascual-Cebrian, E., Skelton, P.W., Gili, E., Salas, R., 2015. Patterns in the distribution of Aptian rudists and corals within a sequence-stratigraphic framework (Maestrat Basin, E Spain). Sedimentary Geology, 321, 86-104.

Bover-Arnal, T., Moreno-Bedmar, J.A., Frijia, G., Pascual-Cebrian, E., Salas, R., 2016. Chronostratigraphy of the Barremian–Early Albian of the Maestrat Basin (E Iberian Peninsula): integrating strontium-isotope stratigraphy and ammonoid biostratigraphy. Newsletters on Stratigraphy, 49, 41-68.

Bover-Arnal, T., Salas, R., Guimerà, J., Moreno-Bedmar, J.A., 2022. Eustasy in the Aptian world: a vision from the eastern margin of the Iberian Plate. Global and Planetary Change, 214, 103849.

Bover-Arnal, T., Guimerà, J., Moreno-Bedmar, J.A, Ferràndez-Cañadell, C., Salas R., 2024. Aptian major changes in accommodation. New sedimentary evidence from the Maestrat Basin (E Iberia). Sedimentary Geology, 459, 106546.

Bulot, L.G., Latil, J.-L., Hairabian, A., Fournillon, A., 2014. New insight on the genus *Nolaniceras* Casey, 1961 (Ammonoidea, Cretaceous) and its consequences on the biostratigraphy of the Aptian Stage. Proceedings of the Geologists' Association, 125, 227-232.

Butler, R.F., 1992. Special topics in rock magnetism. In: Butler, R.F. (ed.). Paleomagnetism: magnetic domains to geologic terranes. Blackwell Sciences Inc., 137pp.

Calvín, P., García-Penas, Á., Zamora, S., Moreno-Bedmar, J.A., Aurell, M., 2024. Paleomagnetic data associated with publication "Latest Barremian - early Aptian chronostratigraphy and sedimentary evolution of the northwestern Maestrat Basin", Geologica Acta. Zenodo. Last Accessed: January 2025. Website: https://doi.org/10.5281/zenodo.14170293

Canérot, J., 1974. Recherches géologiques aux confins des chaines Ibérique et Catalane (Espagne). PhD. Thesis. Tolouse, Université Paul Sabatier, 517pp.

Canérot, J., Cugny, P., Pardo, G., Salas, R., Villena, J., 1982. Ibérica central-Maestrazgo. In: García, A. (ed.). El Cretácico de España. Universidad Complutense de Madrid, 273-344.

Casey, R., 1961. The stratigraphical palaeontology of the Lower Greensand. Palaeontology, 3(4), 487-621.

Casey, R., 1962. A monograph of the Ammonoidea of the Lower Greensand, Part IV. Monograph of the Paleontographical Society, 116, 217-288.

Casey, R., 1964. A monograph of the Ammonoidea of the Lower Greensand, Part V. Monograph of the Palaeontographical Society, 117(1963), 289-398.

Catuneanu, O., Galloway, W.E., Kendall, C.G.St.C., Miall, A.D., Posamentier, H.W., Strasser, A., Tucker, M.E., 2011. Sequence Stratigraphy: Methodology and Nomenclature. Newsletters on Stratigraphy, 44, 173-245. DOI: https://doi.org/10.1127/0078-0421/2011/0011

Clariana, M.P., 1999. Estratigrafía y sedimentología de las facies Urgon (Aptiense) en la subcuenca de Las Parras (Provincia de Teruel). Master Thesis. Zaragoza, Universidad de Zaragoza, 132pp.

Cole, G., Jerret, R., Watkinson, M.P., 2021. A stratigraphic example of the architecture and evolution of shallow water mouth bars, Sedimentology, 68, 1227-1254.

D'Orbigny, A., 1841. Paléontologie française. Description zoologique et géologique de tous les animaux mollusqes et rayonnés fossiles de France. Terrains Crétacés. Vol. 1, Céphalopodes. Part II (1841). Paris, Masson, 121-430.

Delanoy, G., 1995. About some significant ammonites from the Lower Aptian (Bedoulian) of the Angles-Barrême area (South-East France). Memorie Descrittive della Carta Geologica d'Italia, 51, 65-101.

Delanoy, G., 1997. Biostratigraphie des faunes d'Ammonites à la limite Barrémien-Aptien dans la région d'Angles-Barrême-Castellane. Étude particulière de la famille des Heteroceratina Spath, 1922 (Ancyloceratina, Ammonoidea). Annales du Muséum d'Histoire Naturelle de Nice, 12, 1-270.

Delanoy, G., Moreno-Bedmar, J.A., Ruiz, J.J., Tolós Lládser, D., 2013. *Xerticeras* gen. nov., a new genus of micromorphic heteromorph ammonite (Ancyloceratina, Ancyloceratidae) from the lower Aptian of Spain. Carnets de Géologie, Brest, Notebooks on Geology, Article 2013/02 (CG2013_A02), 89-103.

Delanoy, G., Baudouin, C., Pictet, A., Moreno-Bedmar, J.A., Frau, C., Matrion, B., 2022. The genera *Roloboceras* CASEY, 1954, and *Megatyloceras* HUMPHREY, 1949 (Ammonoidea, Ancyloceratina, Douvilleiceratidae), from the Lower Aptian of Ardèche (SE France). Taxonomic and biostratigraphic implications. Carnets de Geology, 22(2), 104pp.

Dutour, Y., 2005. Biostratigraphie, évolution et renouvellements des ammonites de l'Aptien supérieur (Gargasien) du bassin vocontien (Sud-Est de la France). Unpublished doctoral thesis. Université Claude Bernard-Lyon, 1, 302pp.

Embry, A.F., Johannessen, E.P., 1992. T–R sequence stratigraphy, facies analysis and reservoir distribution in the uppermost Triassic–Lower Jurassic succession, western Sverdrup Basin, Arctic Canada. Elsevier, Norwegian petroleum society special publications, 2, 121-146.

Embry, J.-C., Vennin, E., van Buchem, F.S.P., Schroeder, R., Pierre, C., Aurell, M., 2010. Sequence stratigraphy and carbon isotope stratigraphy of an Aptian mixed carbonate-siliciclastic platform to basin transition (Galve subbasin, NE Spain). In: van Buchem, F.S.P., Gerdes, K.D., Esteban, M. (eds.). Mesozoic and Cenozoic Carbonate Systems of the Mediterranean and the Middle East: Stratigraphic and Diagenetic Reference Models. London, The Geological Society, 329 (Special Publications), 113-143.

Fitton, W.H. 1836. Observations on some of the strata between the Chalk and the Oxford Oolite in the south-east of England. Transactions of the Geological Society of London (series 2), 4, 103-390.

Flügel, E., 2010. Microfacies of Carbonate Rocks, Analysis, Interpretation and Application. Berlin, Springer-Verlag, 984pp.

Forbes, E., 1845. Catalogue of Lower Greensand fossils, in the Museum of the Geological Society, with notices of species new to Britain, contained in other Collections. Quarterly Journal of the Geological Society of London, 1, 237-250.

Forner i Valls, E., Moreno-Bedmar, J.A., 2018. *Conulus sanzgarciai* sp. nov. (Echinodermata: Echinoidea) de l'Aptià inferior de Coratxà (conca del Maestrat). Nemus, 8, 69-83.

Frau, C., Delanoy, G., Masse, J.-P., Lanteaume, C., Tendil, A.J.B., 2016. New Heteroceratidae (Ammonoidea) from the Late Barremian deepening succession of Marseille (Bouches–du–Rhône, France). Acta Geologica Polonica, 66, 205-225.

Frau, C., Delanoy, G., Baudouin, C., 2023. A new insight into the lower Aptian Rolobocerati nae Casey, 1961 (Douvilleiceratidae, Ammonoidea) from southern France. Strata, série 2e, 59, 1-21.

Gale, A.S., Mutterlose, J., Batenburg, S., Gradstein, F.M., Agterberg, F.P., Ogg, J.G., Petrizzo, M.R., 2020. The Cretaceous period. In: Gradstein, F.M., Ogg, J.G., Schmitz, M.D., Ogg, G.M. (eds.). Geologic Time Scale 2020. Elsevier, 2, 1023-1086.

Gàmez, D., Paciotti, P., Colombo, F., Salas, R., 2003. The Morella Clay Formation (Lower Aptian), Eastern Iberian Chain (Spain): sedimentological characterization. Geogaceta, 34, 191-194.

García R., Moreno-Bedmar, J.A., 2010. *Dufrenoyia furcata* (Sowerby, 1836) ammonite del Aptiense inferior (Cretácico inferior) del Perelló (Tarragona), Cidaris, 30, 129-138.

García, R., Moreno-Bedmar, J.A., Bover-Arnal, T., Company, M., Salas, R., Latil, J.-L., Martín-Martín, J.D., Gomez-Rivas, E., Bulot, L.G., Delanoy, G., Martínez, R., Grauges, A., 2014. Lower Cretaceous (Hauterivian-Albian) ammonite biostratigraphy in the Maestrat Basin (E Spain). Journal of Iberian Geology, 40(1), 99-112.

García-Mondéjar, J., Owen, H.G., Raisossadat, N., Millán, M.I., Fernández-Mendiola, P.A., 2009. The Early Aptian of Aralar (northen Spain): stratigraphy, sedimentology, ammonite biozonation, and OAE1. Cretaceous Research, 30, 434-464.

García-Penas, Á., Aurell, M., Zamora, S., 2022. Progressive opening of a shallow-marine bay (Oliete Subbasin, Spain) and the record of possible eustatic fall events near the Barremian–Aptian boundary. Palaeogeography, Palaeoclimatology, Palaeoecology, 594, 110938.

García-Penas, Á., Ferratges, F.A., Moreno-Bedmar, J.A., Bover-Arnal, T., Gasca, J.M., Aurell, M., Zamora, S., 2023. Decapod crustaceans from the Lower Cretaceous of Spain, with an account of new occurrences in Barremian–Aptian strata of the Maestrazgo Basin. Cretaceous Research, 105576.

García-Penas, Á., Aurell, M., Zamora, S., 2024. Sedimentary evolution and distribution of benthic fauna of an Aptian protected bay (Oliete Subbasin, Spain). Sedimentary Geology, 461, 106577.

Gautier, F., 1980. Mapa y memoria explicativa de la Hoja núm. 543 (Villarluengo) del Mapa geológico de España 1:50.000. Madrid, Instituto Geológico y Minero de España (IGME), Segunda serie.

Grauges, A., Moreno-Bedmar, J.A., Martínez, R., 2010. Desmocerátidos (Ammonoidea) del Aptiense inferior (Cretácico inferior) de la subcuenca de Oliete, Cordillera Ibérica oriental (Teruel, España). Revista Española de Paleontología, 25(1), 7-18.

Immenhauser, A., Hillgärtner, H., Van Bentum, E., 2005. Microbial-foraminiferal episodes in the Early Aptian of the southern Tethyan margin: ecological significance and possible relation to oceanic anoxic event 1a. Sedimentology, 52, 77-99.

Juárez, M.T., Lowrie, W., Osete, M.L., Meléndez, G., 1998. Evidence of widespread Cretaceous remagnetisation in the Iberian Range and its relation with the rotation of Iberia. Earth and Planetary Science Letters, 160, 729-743.

Luber, T.L., Bulot, L.G., Redfern, J., Frau, C., Arantegui, A., Masrour, M., 2017. A revised ammonoid biostratigraphy for the Aptian of NW Africa: Essaouira-Agadir Basin, Morocco. Cretaceous Research, 79, 12-34.

Martín-Martín, J.D., Gomez-Rivas, E., Bover-Arnal, T., Travé, A., Salas, R., Moreno-Bedmar, J.A., Tomás, S., Corbella, M., Teixell, A., Vergés, J., Stafford, S.L., 2013. The Upper Aptian to Lower Albian syn-rift carbonate succession of the southern Maestrat Basin (Spain): Facies architecture and fault-controlled stratabound dolostones. Cretaceous Research, 41, 217-236.

Martín-Chivelet, J., López-Gómez, J., Aguado, R., Arias, C., Arribas, J., Arribas, M.E., Aurell, M., Bádenas, B., Benito, M.I., Bover-Arnal, T., Casas Sáinz, A., Castro, J.M., Coruña, F. de Gea, G.A., Fornós, J.J., Fregenal-Martínez, M., García-Senz, J., Garófano, D., Gelabert, B., Giménez, J., González-Acebrón, L., Guimerà, J., Liesa, C.L., Mas, R., Meléndez, N., Molina, J.M., Muñoz, J.A., Navarrete, R., Nebot, M., Nieto, L.M., Omodeo-Salé, S., Pedrera, A., Peropadre, C., Quijada, I.E., Quijano, M.L., Reolid, M., Robador, A., Rodríguez-López, J.P., Rodríguez-Perea, A., Rosales, I., Ruiz-Ortiz, P.A., Sàbat, F., Salas, R., Soria, A.R., Suarez-Gonzalez, P., Vilas, L., 2019. The Late Jurassic–Early Cretaceous rifting. In: Quesada, C., Oliveira, J.T. (eds.). The Geology of Iberia: A Geodynamic Approach. Volume 3: The Alpine Cycle. Berlin, Springer, 169-251.

Michel, J., Lanteaume, C., Massonnat, G., Borgomano, J., Tendil, A.J.-B., Bastide, F., Frau, C., Léonide, P., Rebelle, M., Barbier, M., Danquigny, C., Rolando, J.-P., 2023. Questioning carbonate facies model definition with reference to the Lower Cretaceous Urgonian platform (SE France Basin). BSGF - Earth Sciences Bulletin, 194(13), 1-26.

Michelin, H., 1838. Note sur une argile dépendant du Gault, observée au Gaty, commune de Gérodot, département de l'Aube. Mémoires de la Société Géologique de France (series 1), 3, 97-103.

Moreno-Bedmar, J.A., Company, M., Bover-Arnal, T., Salas, R., Delanoy, G., Martínez, R., Grauges, A., 2009. Biostratigraphic characterization by means of ammonoids of the lower Aptian Oceanic Anoxic Event (OAE 1a) in the eastern Iberian Chain (Maestrat Basin, eastern Spain). Cretaceous Research, 30, 864-872.

Moreno-Bedmar, J.A., Company, M., Bover-Arnal, T., Salas, R., Delanoy, G., Maurrasse, F.J.-M.R., Grauges, A., Martínez,

R., 2010a. Lower Aptian ammonite biostratigraphy in the Maestrat Basin (Eastern Iberian Chain, Eastern Spain). A Tethyan transgressive record enhanced by synrift subsidence. Geologica Acta, 8(3), 281-299.

Moreno-Bedmar, J.A., García, R., Salas, R., Ferrer, O., 2010b. Bioestratigrafía de los ammonites del Aptiense inferior (Cretácico Inferior) del Perelló (Tarragona). In: Moreno-Azanza, M., Díaz-Martínez, I., Gasca, J.M., Melero-Rubio, M., Rabal-Garcés, R., Sauqué, V. (coords). VIII Encuentro de Jóvenes Investigadores en Paleontología, volumen de actas. Cidaris, 30, 201-204.

Moreno-Bedmar, J.A., Company, M., Sandoval, J., Tavera, J.M., Bover-Arnal, T., Salas, R., Delanoy, G., Maurrasse, F.J.-M.R., Martínez, R. 2012a. Lower Aptian ammonite and carbon isotope stratigraphy in the eastern Prebetic Domain (Betic Cordillera, southeastern Spain). Geologica Acta, 10(4), 333-350.

Moreno-Bedmar, J.A., Bover-Arnal, T., Barragán, R., Salas, R., 2012b. Uppermost Lower Aptian transgressive records in Mexico and Spain: chronostratigraphic implications for the Tethyan sequences. Terra Nova, 24(4), 333-338.

Moreno-Bedmar, J.A., Barragán, R., Delanoy, G., Company, M., Salas, R., 2014. Review of the early Aptian (Early Cretaceous) ammonoid species Deshayesites deshayesi (d'Orbigny, 1841). Cretaceous Research, 51, 341-360.

Morris, J., 1848. Description of a new species of Nautilus from the Lower Greensand of the Isle of Wight. Annals and Magazine of Natural History, 1, 106-107.

Murat, B., 1983. Contribution à l'étude stratigraphique, sédimentologique et tectonique du Bassin Éocrétacé d'Oliete (Provinde de Teruel, Espagne). PhD Thesis. Tolouse, Université Paul Sabatier, 263pp.

Neres, M., Font, E., Miranda, J.M., Camps, P., Terrinha, P., Mirão, J., 2012. Reconciling Cretaceous palaeomagnetic and marine magnetic data for Iberia: New Iberian palaeomagnetic poles. Journal of Geophysical Research, 117, B06102.

Ossó, À., Moreno-Bedmar, J.A., 2020. A new species of Etyus Leach in Mantell, 1822 (Decapoda, Brachyura, Etidae) from the lower Aptian (Lower Cretaceous) of Cantabria, Spain. Neues Jahrbuch für Geologie und Paläontologie Abhandlungen, 296(1-2), 175-183.

Papp, K., 1907. Beschreibung der während der Forschungsreisen M.V. Déchy im Kaukasus gesammelten Versteinerungen. In: Déchy, M.V. Kaukasus III. Reisen und Forschungen im Kaukasischen Hochgebirge, 141-173.

Peropadre, C., 2012. El Aptiense del margen occidental de la Cuenca del Maestrazgo: controles tectónico, eustático y climático en la sedimentación. PhD Tesis. Universidad Complutense de Madrid, 649pp.

Peropadre, C., Meléndez, N., Liesa, C.L., 2012. Nuevas unidades estratigráficas del Aptiense en la cuenca del Maestrazgo (este de España). Geo-Temas, 13, 147-150.

Peropadre, C., Liesa, C.L., Meléndez, N., 2013. High-frequency, moderate to high- amplitude sea-level oscillations during the late Early Aptian: insights into the mid- Aptian event (Galve sub-basin, Spain). Sedimentary Geology, 294, 233-250.

Pictet, F.J., 1847. Description des mollusques fossiles qui se trouvent dans le Gres Vers des environs de Geneve. Mémoires de la Société de Physique et d'Histoire Naturelle de Genève, 11, 257-412.

Rameil, N., Immenhauser, A., Warrlich, G., Hillgärtner, H., Droste, H.J., 2010. Morphological patterns of Aptian Lithocodium-Bacinella geobodies: relation to environment and scale. Sedimentology, 57, 883-911.

Reboulet, S., Hoedemaeker, P.J., Aguirre-Urreta, M.B., Alsen, P., Atrops, F., Baraboshkin, E.Y., Company, M., Delanoy, G., Dutour, Y., Klein, J., Latil, J-.L., Lukeneder, A., Mitta, V., Mourgues, F.A., Ploch, I., Raisossadat, N., Ropolo, P., Sandoval, J., Tavera, J.M., Vasicek, Z., Vermeulen, J., 2006. Report on the 2nd international meeting of the IUGS lower Cretaceous ammonite working group, the "Kilian Group" (Neuchâtel, Switzerland, 8 September 2005). Cretaceous Research, 27, 712-715.

Reboulet, S., Rawson, P.F., Moreno-Bedmar, J.A., Aguirre-Urreta, M.B., Barragán, R., Bogomolov, Y., Company, M., González-Arreola, C., Stoyanova, V.I., Lukeneder, A., Matrion, B., Mitta, V., Randrianaly, H., Vašiček, Z., Baraboshkin, E.J., Bert, D., Bersac, S., Bogdanova, T.N., Bulot, L.G., Latil, J.-L., Mikhailova, I.A., Ropolo, P., Szives, O., 2011. Report on the 4th International Meeting of the IUGS Lower Cretaceous Ammonite Working Group, the "Kilian Group" (Dijon, France, 30th August 2010). Cretaceous Research, 32, 786-793.

Ropolo, P., Conte, G., Moullade, M., Tronchetti, G., Gonnet, R., 2008. The Douvilleiceratidae (Ammonoidea) of the Lower Aptian historical stratotype area at Cassis-La Bédoule (SE France). Brest, Carnets de Géologie/Notebooks on Geology, Memoir 2008/03 (CG2008_M03), 1-60.

Rouchadzé, I., 1933. Les ammonites aptiennes de la Géorgie occidentale. Bulletin de l'Institut géologique de Géorgie, 1(3), 165-273.

Salas, R., 1987. El Malm i el Cretaci inferior entre el Massís de Garraf i la Serra d'Espadà. Anàlisi de Conca. PhD Thesis. Barcelona, Universitat de Barcelona, 541pp.

Salas, R., Casas, A., 1993. Mesozoic extensional tectonics, stratigraphy, and crustal evolution during the Alpine cycle of the eastern Iberian basin. Tectonophysics, 228, 33-55.

Salas, R., Guimerà, J., 1996. Rasgos estructurales principales de la cuenca cretácica inferior del Maestrazgo (Cordillera Ibérica oriental). Geogaceta, 20, 1704-1706.

Salas, R., Martín-Closas, C., Querol, X., Guimerà, J., Roca, E., 1995. Evolución tectonosedimentaria de las cuencas del Maestrazgo y Aliaga-Penyagolosa durante el Cretácico Inferior. In: Salas, R., Martín-Closas, C. (eds.). El Cretácico inferior del Nordeste de Iberia. Barcelona, Universitat de Barcelona, 13-94.

Salas, R., Guimerà, J., Mas, R., Martín-Closas, C., Meléndez, A., Alonso, A., 2001. Evolution of the Mesozoic Central Iberian Rift System and its Cainozoic inversion (Iberian Chain). In: Ziegler, P.A., Cavazza, W., Roberston, A.H.F., Crasquin-Soleau, S. (eds.). Peri-Tethys Memoir 6: Peri-Tethyan Rift/

Wrench Basins and Passive Margins. Paris, Mémoires du Muséum National d'Histoire Naturelle, 186, 145-186.

Soria, A.R., 1997. La sedimentación en las cuencas marginales del Surco Ibérico durante el Cretácico Inferior y su contorno estructural. Ph.D. Thesis. Zaragoza (Spain), Universidad de Zaragoza, 363pp.

Soria, A.R., Vennin, E., Meléndez, A., 1994. Estratigrafía, sedimentología y control tectónico en la evolución de las rampas carbonatadas del Cretácico Inferior de la Cubeta de Oliete (provincia de Teruel). Revista de la Sociedad Geológica de España, 7, 47-61.

Sornay, J., Marin, P., 1972. Sur la faune d'ammonites aptiennes de la Tejeria de Josa (Teruel, Espagne). Annales de Palaeontologie, 63, 101-123.

Sowerby, J. de C., 1836. Appendix A: Descriptive notes respecting the shells figured in pl. 11 to 23, (pp. 335-348). In: Fitton, W.H. (ed.). Observations on some of the strata between the Chalk and the Oxford Oolite in the south-east of England. Transactions of the Geological Society of London (series 2), 4, 103-390.

Spath, L.F., 1930. On some Ammonoidea from the Lower Greensand. Annals and Magazine of Natural History (series 10), 5, 417-464.

Strasser, A., 1986. Ooids in Purbeck limestones (lowermost Cretaceous) of the Swiss and French Jura. Sedimentology, 33, 711-727.

Szives, O., Latil, J.-L., Moreno-Bedmar, J.A., Lehmann, J., Robert, E., Owen, H.G., 2023. Critical revision and new proposals on the Aptian-Albian zonation of the Standard Mediterranean Ammonite Zonal Scheme. Newsletters on Stratigraphy, 56(4), 423-456.

Szives, O., Moreno-Bedmar, J.A., Aguirre-Urreta, B., Company, M., Frau, C., López-Horgue, M., Pictet, A., Ploch, I., Salazar, C., Barragán, R., Latil, J.L., Lehmann, J., Robert, E., Reboulet, S., 2024. Report on the 7th International Meeting of the IUGS Lower Cretaceous Ammonite Working Group, the Kilian Group (Warsaw, Poland, 21st August 2022): State of the art on the current Standard Ammonite Zonation of the Western Tethyan Mediterranean Province. Cretaceous Research, 153, 105716.

Védrine, S., Strasser, A., Hug, W., 2007. Oncoid growth and distribution controlled by sea-level fluctuations and climate (Late Oxfordian, Swiss Jura Mountains). Facies, 53, 535-552.

Vennin, E., Soria de Miguel, A., Preat, A., Meléndez Hevia, A., 1993. Análisis secuencial durante el intervalo Barremiense-Aptiense en la Cubeta de Oliete. Cuadernos de Geología Ibérica, 17, 257-283.

Vennin, E., Aurell, M., 2001. Stratigraphie sequentielle de l'Aptien du sous-bassin de Galve (Province de Teruel, NE de l'Espagne). Bulletin de la Société Géologique de France, 172, 397-410.

Manuscript received June 2024;
revision accepted December 2025;
published Online January 2025.

APPENDIX I

TABLE I. Stratigraphic features and components of the different facies identified in the studied succession

	Sedimentary features	Key components
(F1) Mudstones and silty limestones with laminated sandstone interbeds	Meter to decameter-thick tabular levels of white, blue–grey or ochreish clay with mm-thick silty interbeds, and cm-thick interbeds of fine quartz sand with hummocky and planar cross-lamination	Discoidal orbitolinids, solitary corals, regular and irregular echinoids. Abundant decapod crustaceans, occasionally in carbonate concretions. Scarce ammonoids and nautiloids. Scarce teeth of small shark and durophagous fishes; ostracods, small bivalves (pectinids, gryphaeid oysters). Quartz sand, muscovite, diagenetic gypsum.
(F2) Gray to ochreish mudstones with bioclastic limestone interbeds	Meter to decameter-thick massive beds of marls with interbedded nodulose bioclastic packstones.	Orbitolinids, regular and irregular echinoids, bivalves, gastropods, occasional colonial corals. Rare ammonites. In limestone interbeds: abundant instraclasts, peloids, ostracods, fragments of molluscs, brachiopods, bryozoans, echinoids and green algae. Quartz sand.
(F3) Gray and blue mudstones with bioclastic marly limestone interbeds	Meter to decameter-thick massive beds of marls with interbedded nodulose bioclastic limestone.	Ammonites, nautiloids, pectinid bivalves (including *Plicatula sp.*), gryphaeid oysters (*Ceratostreon sp.*), other unidentified bivalves, gastropods, brachiopods (rhynchonellids, terebratulids) foraminifera, green alge, fish teeth, decapod crustaceans, regular and irregular echinoids. Frequent *Thalassinoides* isp. in the limestones. Occasionally fine quartz sand, glauconite.
(F4) Orbitolinid wackestone-packstone	Decimeter to meter-thick beds with nodular (bioturbated) bedding.	Flattened and conical orbitolinids, other textulariids (including *Choffatella*), occasional miliolids. Unidentified bivalves and gastropods. In the Oliete subbasin: frquent green algae and decapod crustacean debris. Occasionally fine quartz sand.
(F5) Orbitolinid sandstone	Decimetric tabular beds.	Large discoidal orbitolinids. Diverse benthic foraminifera, solitary corals, calcispheres, ostracods, tiny gastropods. Echinoid plates and spicules. Debris of serpulids, oysters and decapod crustaceans. Fine quartz sand.

TABLE I. Continued

	Sedimentary features	Key components
(F6) Bioclastic grainstones with large-scale planar cross-bedding	Meter-thick beds of bioclastic limestones with Planar cross-bedding, and horizontal beds of bioturbated bioclastic packstones. Occasionally, dolomitisation and dissolution vugs.	Abraded fragments of bivalves, gastropods, brachiopods, bryozoans, green and red algae, echinoids, decapod crustaceans, ostracods, serpulids. Abundant intraclasts of bioclastic wackestone, micrite, and ooidal packstone-grainstone. Abundant cortoids with constructive and destructive coatings. Glauconite.
(F7) Ooid-bioclastic packstones to grainstones	Decimeter to meter-thick beds, frequently with planar cross-bedding.	Abraded well-sorted fragments of molluscs, bryozoans, brachiopods and green algae, abundant benthic foraminifera (miliolids, small agglutinated forms). Abundant type 1 ooids (Strasser, 1986), sometimes forming aggregate grains. Cortoids with constructive and destructive coatings.
(F8) Ooid grainstones	Decimeter to meter-thick beds with planar cross bedding, or internal planar cross lamination.	Very rare rounded bioclasts and small agglutinated benthic foraminifera. Well sorted type-1 ooids, occasionally forming aggregate grains.
(F9) Intraclastic grainstones	Decimeter to meter-thick tabular beds with massive bedding or planar cross-bedding.	Partly micritized and rounded fragments of oysters and other indeterminate molluscs. Orbitolinids, fragments of green algae, echinoids, bryozoans and serpulids. Intraclasts of mud-supported facies, including peloidal packstones with benthic foraminifera, bioclastic packstones and bioclastic-ooidal packstones.
(F10) Cortoid packstone-grainstone	Decimeter to meter-thick beds with planar cross-bedding.	Skeletal debris of oysters and other unidentified bivalves. Cortoids with destructive and constructive coatings, intraclasts, peloids.
(F11) Oyster bioclastic grainstones	Meter-thick beds with planar cross-bedding.	Abraded oyster fragments, disarticulated echinoid and crinoid elements. Other unidentifiable bioclasts. Locally, pervasive dolomitisation and abundant dissolution vugs.
(F12) Oncoid wackestone-packstone	Decimeter to meter-thick, irregular bedding. Bioturbated.	Scarce mollusc bioclasts. Type 3 oncoids (Védrine et al, 2007) with bioclastic nucleii, including mostly fragments of colonial corals, molluscs.

TABLE I. Continued

	Sedimentary features	Key components
(F13) Mudstones and peloidal-foraminiferal wackstones to grainstones	Decimeter to meter-thick massive bedding	Very abundant and diverse small benthic foraminifera, including abundant miliolids and, orbitolinids; ostracods, green algae fragments. Cortoids with destructive coatings, sometimes almost fully micritized; poorly sorted peloids, intraclasts, aggregate grains. Rare type 1 ooids.
(F14) Coral-*Lithocodium* bindstone	Decimeter to meter-thick beds with nodulose bedding.	Massive tabular buildups of whole corals and coral debris encrusted by *Lithocodium*. Orbitolinids, serpulids, and variable proportions of indeterminate skeletal debris.
(F15) Rudist-coral floatstone	Meter-thick massive beds.	Scattered articulated and disarticulated rudists and colonial corals in a micritic matrix.
(F16) Mudstones-packstones with restricted-marine fauna and/or root traces	Centimeter to decimeter-thick tabular levels, sometimes with nodulose (bioturbated) bedding. Occasional root traces.	Massive accumulations of ostracods. Gastropods, thin-shelled bivalves. Scarce oysters. Rare charophyte gyrogonites. Quartz sand, muscovite.

APPENDIX II

PALEOMAGNETISM

Methods

Paleomagnetic sampling was conducted along the Alacón Fm. in the Alacón (AL) and Barranco del Moro (BM) logs. The lowermost section of the Alacón Formation is located at 41.020917°N, 0.685157°W (ETRS89), while the lowermost section of the Barranco del Moro Formation is situated at 40.990780°N, 0.601061°W (ETRS89). A total of 50 m of stratigraphic series (Table II) and 31 levels (with one sample taken per level) were initially sampled along the AL profile in a 1-2m interval. Twenty-one additional samples were obtained from the upper part of the section (between meters 24 to 50) in a second field campaign to reinforce the interpretation of the critical area of the section. A total of 47 levels were sampled within the 30-meter thick BM sections (Table II).

Samples were cut into one to three standard palaeomagnetic specimens at the Palaeomagnetic Laboratory of the University of Burgos, where both Thermal (Th) and Alternating Field (AF) demagnetization was performed using a 755 cryogenic magnetometer (2G) equipped with AF coils and a TD48-DC thermal demagnetizer (ASC scientific). Th demagnetization was performed on 87 specimens (52AL and 35BM) using a stepwise procedure with 10 to 13 steps in a 30-125ºC step interval up to 575ºC. AF demagnetization was performed two specimens in the AL section were Th experiments gave the best results, while 29BM specimens were demagnetized by AF were a combination of Th and AF demagnetizations was the best laboratory protocol to obtain a reliable record.

Characteristic Remanent Magnetization (ChRM) was calculated by principal component analysis (Kirschvink, 1980) using the Remasoft software (Chadima and Hrouda, 2006) and ChRM directions were processed using Stereonet software (Cardozo and Allmendinger, 2013). A stability test (bootstrapping reversal and fold test) was performed using PmagPy software (Tauxe *et al.*, 2018). Calculated ChRM from Th experiments were classified from quality 1 to 3 (being 1 the best paleomagnetic quality) and Virtual Geomagnetic Poles (VGP) were calculated (Butler, 1992) per specimen from bedding corrected ChRM. Quality 1 Th directions and AF directions were used to establish the local polarity sequence.

Palaeomagnetic components and stability tests

The ChRM from thermal experiments was isolated in 41 and 33 specimens from AL and BM logs, respectively, for a total of 74 ChRM directions, while 24 AF directions were calculated from BM specimens. The Natural Remanent Magnetization (NRM) of the measured specimens ranges from 0.033 to 30mA/m, with a mean of 1.75mA/m and a standard deviation of 3.98mA/m (Fig. IA). ChRM shows maximum values of 0.003 and 0.4mA/m, with a mean value of 0.066mA/m and a standard deviation of 0.074mA/m (Fig. 4A). ChRM and NRM intensities are not related, and variable rations between 2 and 22 are derived from them (Fig. IA).

The ChRM in Th demagnetization has been separated into three different qualities based on their palaeomagnetic behaviour (Fig. IB-D), which are observed independently either of the polarity of the palaeomagnetic direction or the intensity of the NRM. Quality 1 (Fig. IB) is defined as ChRM calculated from three or more temperature steps, and the calculated palaeomagnetic component goes to the origin. In quality 2 (Fig. IC), however, the palaeomagnetic component is also calculated with three or more temperature steps but the component does not go to the origin. Unblocking temperatures for both quality 1 and 2 are between 250/350 and 450/575ºC. Finally, quality 3 (Fig. ID) is characterised by the presence of a cluster between 250/350 to 400/500ºC that shows clear polarity but is not demagnetized, and therefore the palaeomagnetic component is calculated by forcing to the origin.

The ChRM is well defined in most of the specimens with qualities 1 and 2. On the other hand, AF demagnetizations show two types of behaviour independently of the quality in Th demagnetization. In some specimens, such as BM20-01A (Fig. IB-D), NRM is mostly demagnetized after 100mT and two palaeomagnetic components can be isolated. The low coercivity component has unblocking coercivities ranging from 0 to 10mT and indicates a recent overprint since the calculated direction point to the N with a positive inclination Before Bedding Correction (BBC). The high coercivity component is isolated between 20/60 and 100mT and shows the same direction as the ChRM isolated in thermal experiments (Fig. IB-D). The second behaviour observed in AF demagnetizations (Fig. IE) is characterised by NRM carried by ferromagnetic s.l. minerals with coercivities above 100mT since more than the 60/80% of the NRM is not demagnetized after the final AF step. Palaeomagnetic directions with this behaviour

have been discarded because when a palaeomagnetic component with the coercivity spectra of 20/60-100mT (similar to the previous behaviour) is calculated, it presents randomly distributed directions (Fig. IE). The most likely carrier of the palaeomagnetic component is magnetite, given the unblocking temperatures and coercivities of the ChRM, while goethite and hematite are also present in the studied samples.

Out of the 98ChRM calculated directions, 74 were obtained from Th demagnetizations and 24 from AF demagnetizations. After removing directions with maximum angular deviations above 20º and the palaeomagnetic components with the second behaviour in AF experiments (Fig. 4E), 79 directions were used in the following procedures (Fig. II). For the AL log, 36 palaeomagnetic directions were used, consisting of 22 quality 1 directions and seven quality 2 and 3 directions. The BM log utilized 43 directions, including 14 quality 1 directions, nine quality 2 directions, six quality 3 directions and 14 directions from AF demagnetizations. Palaeomagnetic directions show a better clustering (Fig. IIA, main text) after than before bedding correction (ABC and BBC respectively), which is consistent with the fold-test results that show the best clustering after a 78-101% unfolding (Fig. IIB). Mean palaeomagnetic directions were calculated for normal, reversed, and normal plus reversed polarities. The directions shown are similar to each other, resulting in a positive reversal test (Fig. IIB), as well as to the mean expected directions for 100-130Ma (Neres *et al.*, 2012). However, the inclinations are lower, which could be attributed to the shallowing effect. The positive reversal and fold-test (Fig. IIB) support the primary origin of the ChRM.

REFERENCES

Butler, R.F., 1992. Palaeomagnetism: Magnetic Domains to Geologic Terranes. Blackwell Scientific Publications, 319pp.

Cardozo, N., Allmendinger, R.W., 2013. Spherical projections with OSXStereonet. Computers and Geosciences, 51, 193-205. DOI: https://doi.org/10.1016/j.cageo.2012.07.021

Chadima, M., Hrouda, F., 2006. Remasoft 3.0 a user-friendly palaeomagnetic data browser and analyzer. Travaux Géophysiques, 27, 20-21.

Kirschvink, J.L., 1980. The least-squares line and plane and the analysis of palaeomagnetic data. Geophysical Journal of the Royal Astronomical Society, 62, 699-718. DOI: https://doi.org/10.1111/j.1365-246X.1980.tb02601.x

Neres, M., Font, E., Miranda, J.M., Camps, P., Terrinha, P., Mirão, J., 2012. Reconciling Cretaceous palaeomagnetic and marine magnetic data for Iberia: New Iberian palaeomagnetic poles. Journal of Geophysical Research, 117, B06102.

Tauxe, L., Shaar, R., Jonestrask, L., Swanson-Hysell, N.L., Minnett, R., Koppers, A.A.P., Constable, C.G., Jarboe, N., Gaastra, K., Fairchild, L., 2016. PmagPy: Software package for palaeomagnetic data analysis and a bridge to the Magnetics Information Consortium (MagIC) Database. Geochemistry, Geophysics, Geosystems, 17, 2450-2463. DOI: https://doi.org/10.1002/2016GC006307

TABLE I. Coordinates of referenced logs (ETRS89)

	Section name	Coordinates base	Coordinates top
Oliete Subbasin	Alacón AL	0° 40' 37.48" W,41° 01' 45.87" N	0° 40' 49.25" W,41° 00' 55.39" N
	Barranco del Moro BM	0° 36' 04.83" W,40° 59' 26.63" N	0° 36' 01.39" W,40° 59' 29.87" N
	Estercuel ES	0° 39' 03.32" W,40° 50' 18.45" N	0° 38' 33.62" W,40° 50' 34.04" N
	Gargallo GG	0° 34' 59.98" W,40° 50' 31.18" N	0° 34' 52.96" W,40° 50' 37.16" N
	Obón OB	0° 44' 20.46" W,40° 54' 57.79" N	0° 44' 22.27" W,40° 54' 35.05" N
	Tejería de Josa JO	0° 46' 38.08" W,40° 57' 18.16" N	0° 46' 44.37" W,40° 57' 31.38" N
Morella Subbasin	Barranco de los Degollados BD	0° 33' 15.40" W,40° 42' 42.33" N	0° 33' 16.48" W,40° 42' 39.06" N
	Berge BG	0° 27' 56.51" W,40° 51' 07.01" N	0° 27' 55.03" W,40° 51' 10.78" N
	Bordón BO	0° 19' 13.31" W,40° 41' 41.71" N	0° 19' 11.24" W,40° 41' 34.20" N
	Cantavieja CV1	0° 23' 54.77" W,40° 31' 11.73" N	0° 24' 15.23" W,40° 31' 49.89" N
	Cantavieja 2 CV2	0° 23' 30.18" W,40° 33' 09.72" N	0° 23' 34.77" W,40° 33' 11.70" N
	Cañada de Benatanduz CB	0° 33' 45.60" W,40° 36' 11.42" N	0° 33' 47.42" W,40° 36' 03.91" N
	Castellote CS	0° 19' 05.33" W,40° 47' 22.45" N	0° 18' 55.05" W,40° 47' 17.75" N
	Jaganta JG	0° 16' 20.66" W,40° 46' 59.22" N	0° 16' 14.15" W,40° 46' 56.38" N
	Ladruñán LA	0° 22' 46.32" W,40° 44' 31.03" N	0° 22' 31.31" W,40° 44' 28.14" N
	Mola de la Garumba MG	0° 11' 31.60" W,40° 37' 57.83" N	0° 11' 10.50" W,40° 38' 05.87" N
	Olocau del Rey OL	0° 20' 26.18" W,40° 37' 53.69" N	0° 20' 26.78" W,40° 38' 02.49" N
	Villores	0° 15' 13.23" W,40° 41' 33.64" N	0° 15' 15.75" W,40° 41' 34.55" N

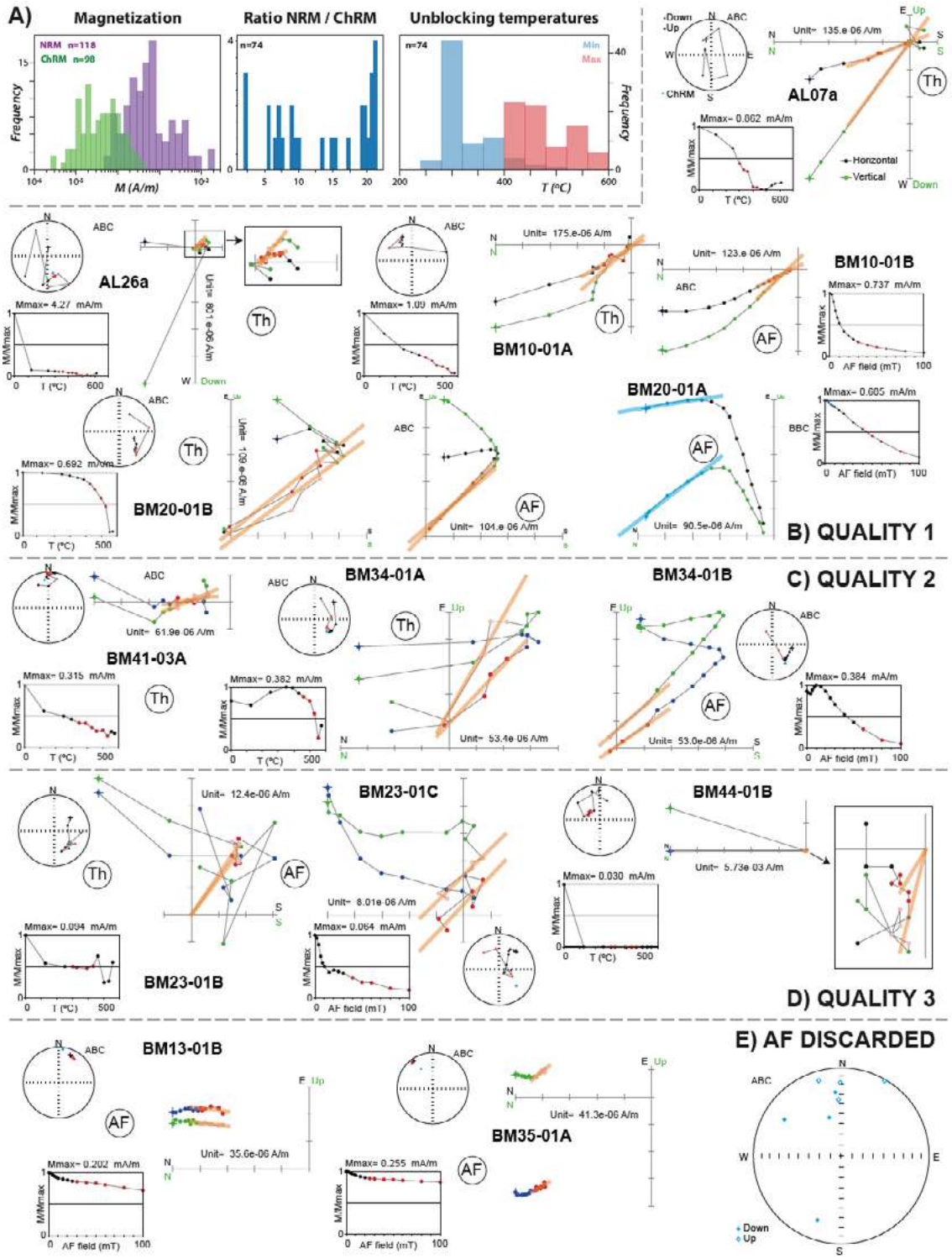

FIGURE I. A) Histograms with the intensity of the NRM and the ChRM, as well as their respective ratios, and the minimum and maximum unblocking temperatures. B, C, D) Thermal (Th) and alternating field (AF) demagnetization diagrams of representative specimens for qualities 1, 2 and 3 respectively, displaying thermal (Th) and alternating field (AF) demagnetizations of the NRM with the used steps (in pink/red) used to calculate the ChRM. The plots showing the intensity decay and the equal-area projections (lower hemisphere) showing the directions of the individual demagnetization steps are also shown. All plots are in restored coordinates (after bedding correction, ABC), except for BM20-01A, which is in geographic coordinates (before bedding correction, BBC). E) Orthogonal plots of the AF demagnetization of the NRM of two specimens and an equal area stereoplot with the derived ChRM directions illustrating the second (and discarded) behavior found in the AF demagnetizations (see text for further details).

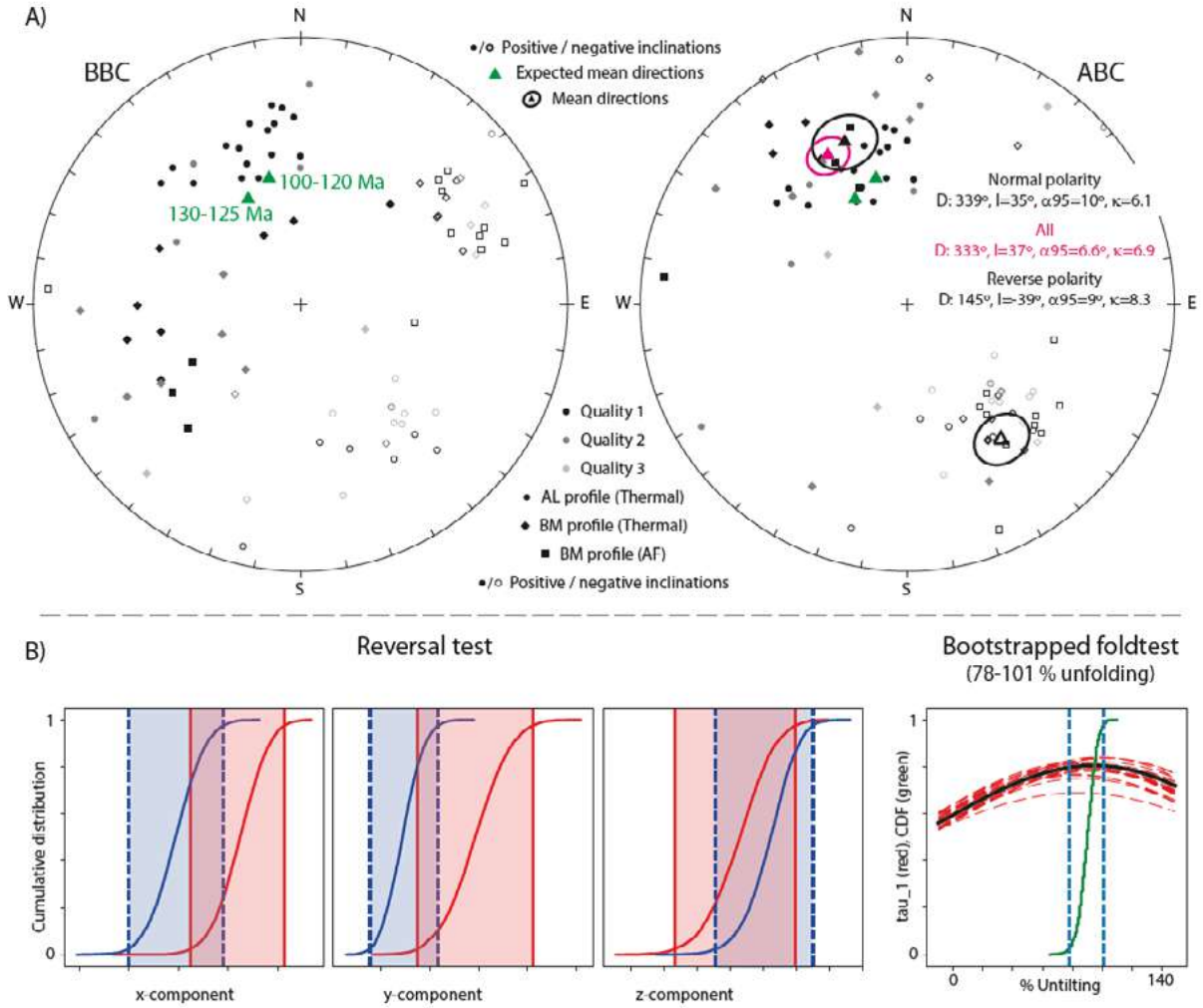

FIGURE II. A) Equal-area stereographic projection (lower hemisphere) showing the ChRM directions before and after bedding correction (BBC and ABC respectively). The mean direction and statistical parameters (Fisher, 1953) were calculated for ABC directions considering only normal or reversal populations, and also considering all directions together after rotating the reversals to the normal position. B) Reversal and bootstrapped foldtest (Tauxe *et al.*, 2018) that support a primary origin of the ChRM.

TABLE II. Position along each profile of the sampled paleomagnetic samples. Quality of thermal CHM directions or calculated AF directions is also indicated

BM section			AL Section		
Site	**Thickness (m)**	**Quality**	**Site**	**Thickness (m)**	**Quality**
AL01	0.9		BM02	4	
AL02	4.4	2	BM03	4.8	1
AL03	5.2	1	BM04	5.6	1
AL04	5.7	1	BM05	6	
AL05	6.6	1	BM06	7.3	
AL06	8	1	BM07	8	1
AL07	8.1	1	BM08	9.5	2
AL08	9.1	2	BM09	10	2
AL09	10.7	1	BM10	10.3	1
AL10	12.9	1	BM11	10.6	AF
AL11	13.6	1	BM12	11	
AL12	14.1	1	BM13	12	2
AL13	17.1		BM14	12.5	2
AL14	19.3	1	BM15	13	3
AL15	20.8	1	BM16	13.2	
AL16	24.5		BM17	13.5	1, AF
AL40	24.5	1	BM18	14	AF
AL17	25.9	1	BM19	15	1
AL41	25.9	1	BM20	15.2	1, AF
AL18	27.1	1	BM21	15.5	3
AL44	27.1	2	BM22	15.8	1
AL43	28	1	BM23	16	3, AF
AL19	28.1		BM24	16.2	1
AL42	28.2	2	BM25	16.4	
AL45	32		BM26	16.5	1, AF
AL46	32.5		BM27	16.5	
AL20	32.8		BM28	16.7	AF
AL47	33.2	3	BM29	16.8	
AL21	33.9		BM30	16.9	3, AF
AL48	35.9	3	BM31	17	
AL22	36.7		BM32	17.2	
AL49	37.1	3	BM33	17.4	AF
AL23	38		BM34	17.5	2, AF
AL50	38	3	BM35	18	
AL51	38.2		BM36	19.2	2, AF
AL24	39.5		BM37	19.6	3
AL52	39.5	1	BM38	20	
AL25	40		BM39	20.5	2, AF
AL53	42.8		BM40	22	1
AL26	44.8	1	BM41	22.1	2, AF
AL27	44.9		BM42	24	
AL54	44.9	1	BM43	28	2
AL28	45.9		BM44	28.1	3
AL55	45.9	1, 2	BM45	28.3	
AL56	47.8	1	BM46	29	1
AL57	47.8	1	BM47	29.5	
AL58	48.1	3	BM48	30	1
AL29	49.5				
AL59	49.5	3			
AL30	49.9	2			
AL60	50.1	2			
AL31	51.1	3			

APPENDIX III

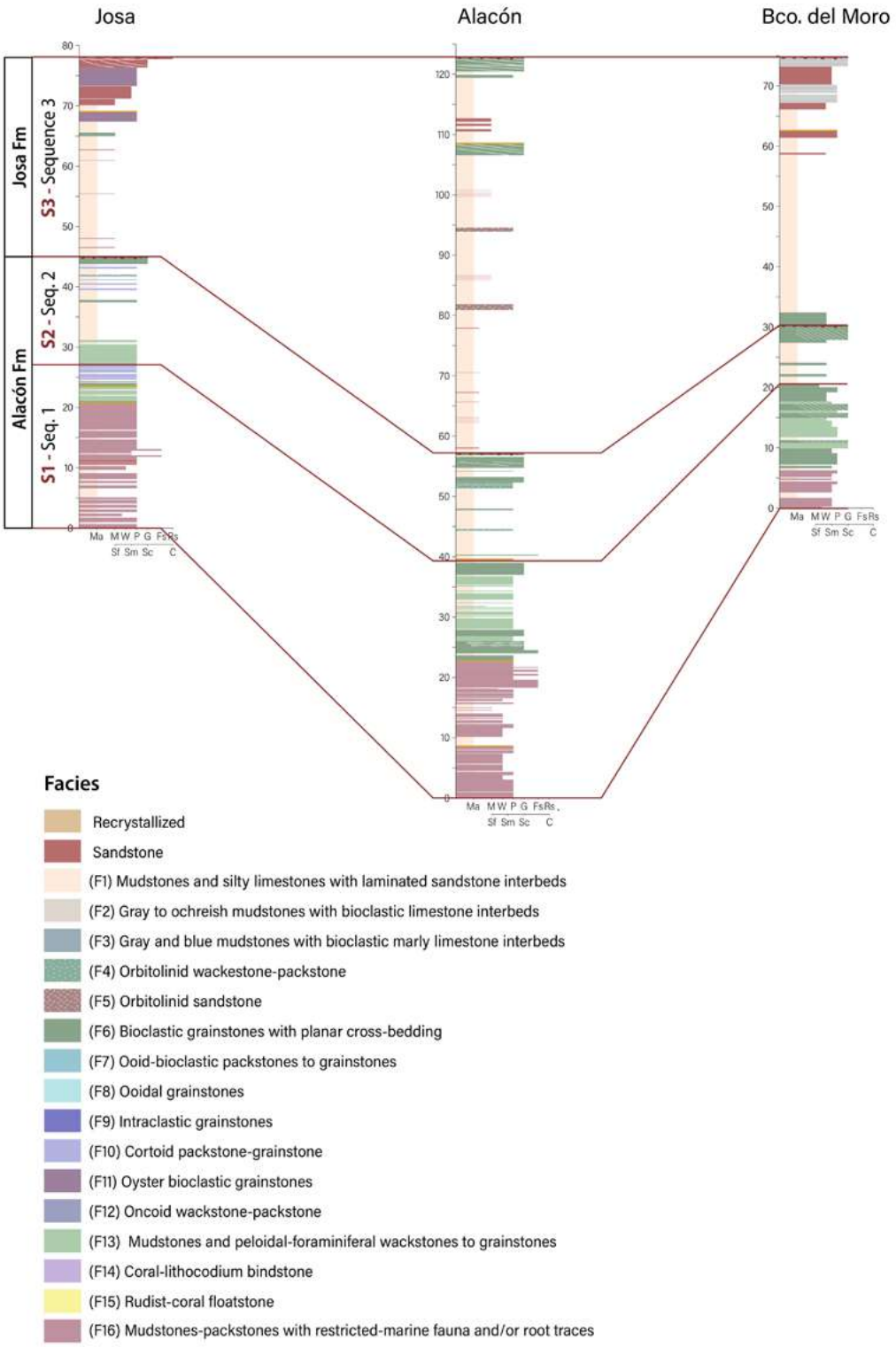

FIGURE III.

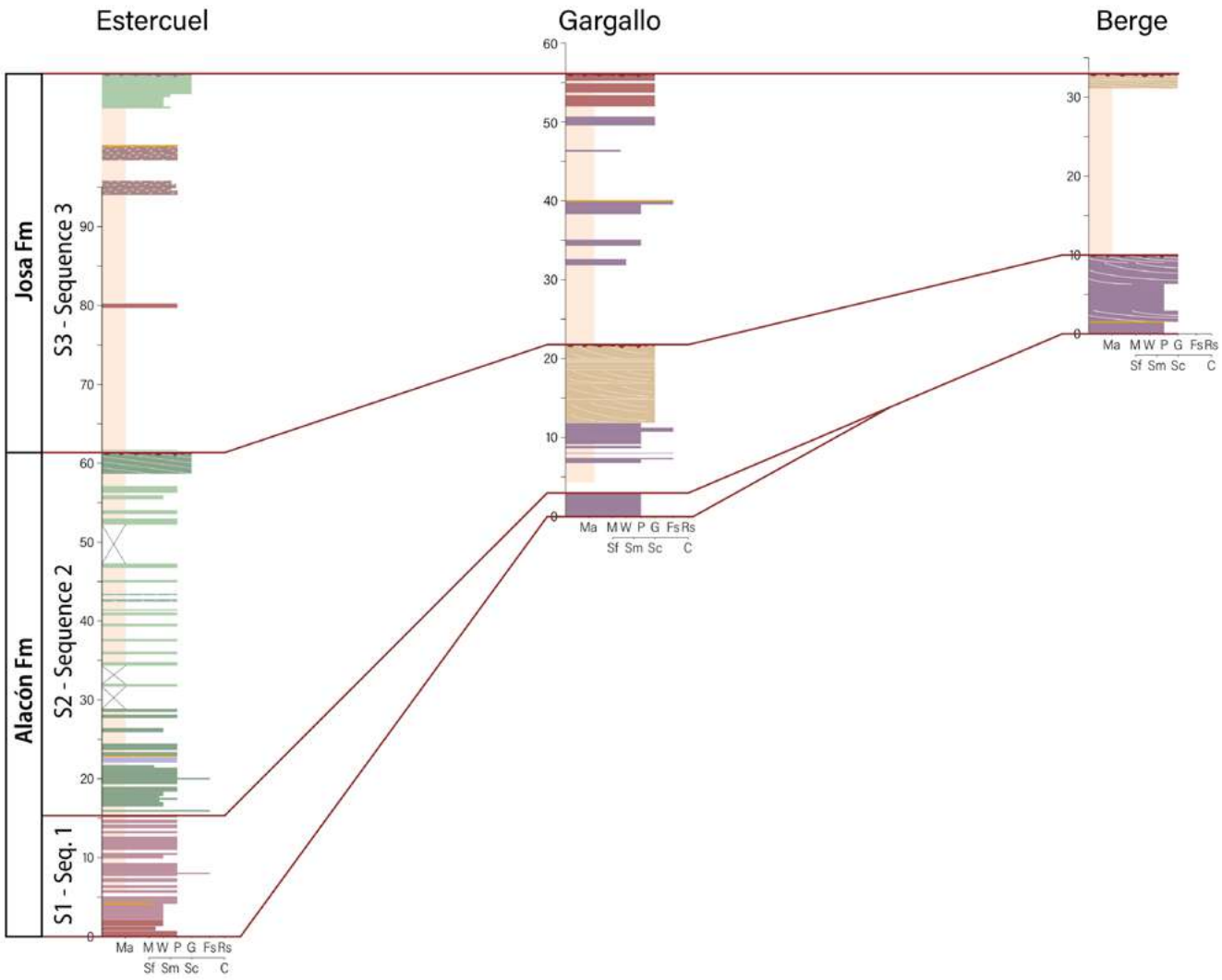

FIGURE IV.

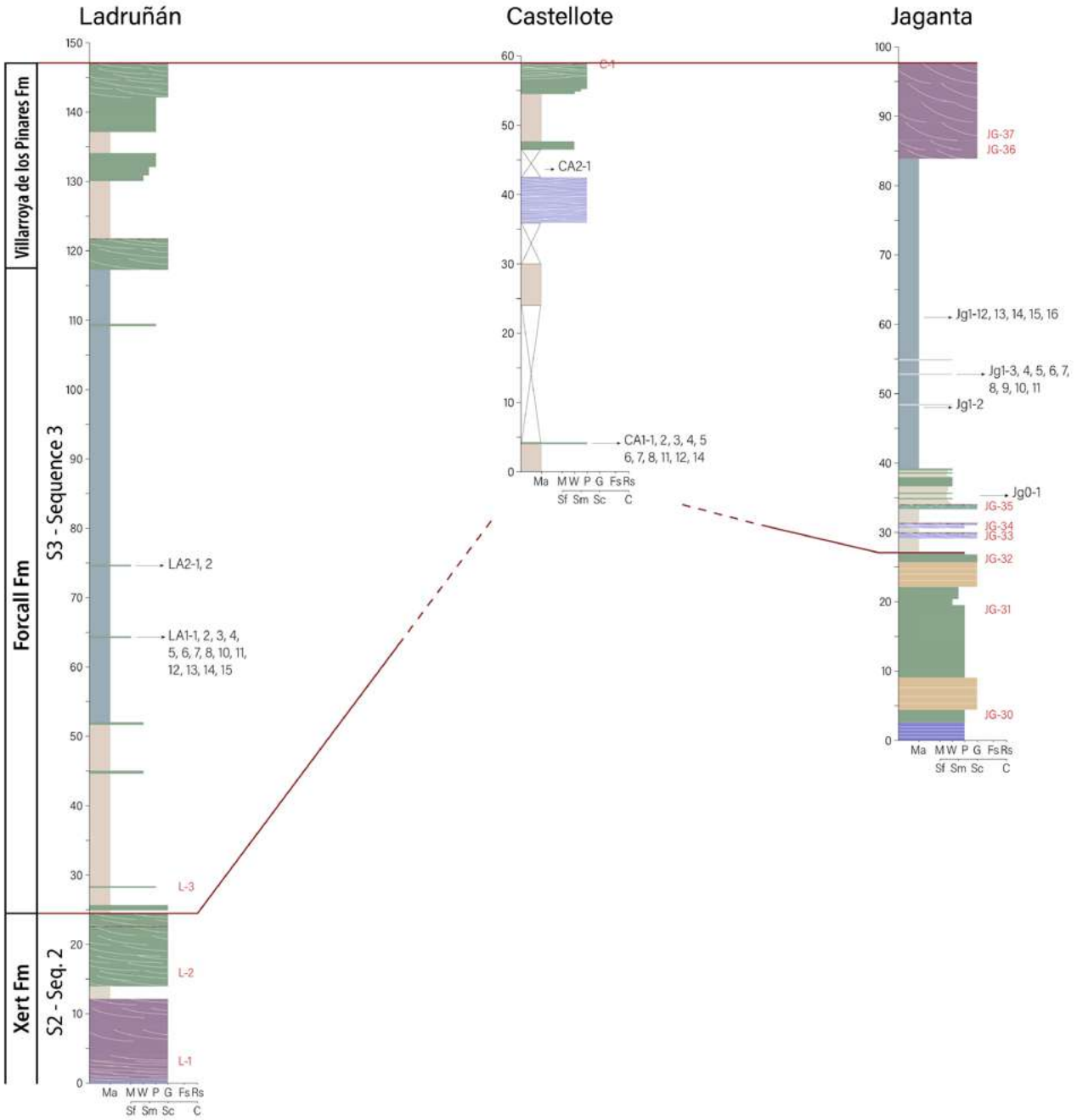
Ladruñán
Castellote
Jaganta
Villarroya de los Pinares Fm
Forcall Fm
Xert Fm
S3 - Sequence 3
S2 - Seq. 2
LA2-1, 2
LA1-1, 2, 3, 4, 5, 6, 7, 8, 10, 11, 12, 13, 14, 15
L-3
L-2
L-1
C-1
CA2-1
CA1-1, 2, 3, 4, 5 6, 7, 8, 11, 12, 14
JG-37
JG-36
Jg1-12, 13, 14, 15, 16
Jg1-3, 4, 5, 6, 7, 8, 9, 10, 11
Jg1-2
Jg0-1
JG-35
JG-34
JG-33
JG-32
JG-31
JG-30
Ma M W P G Fs Rs
Sf Sm Sc C

FIGURE V.

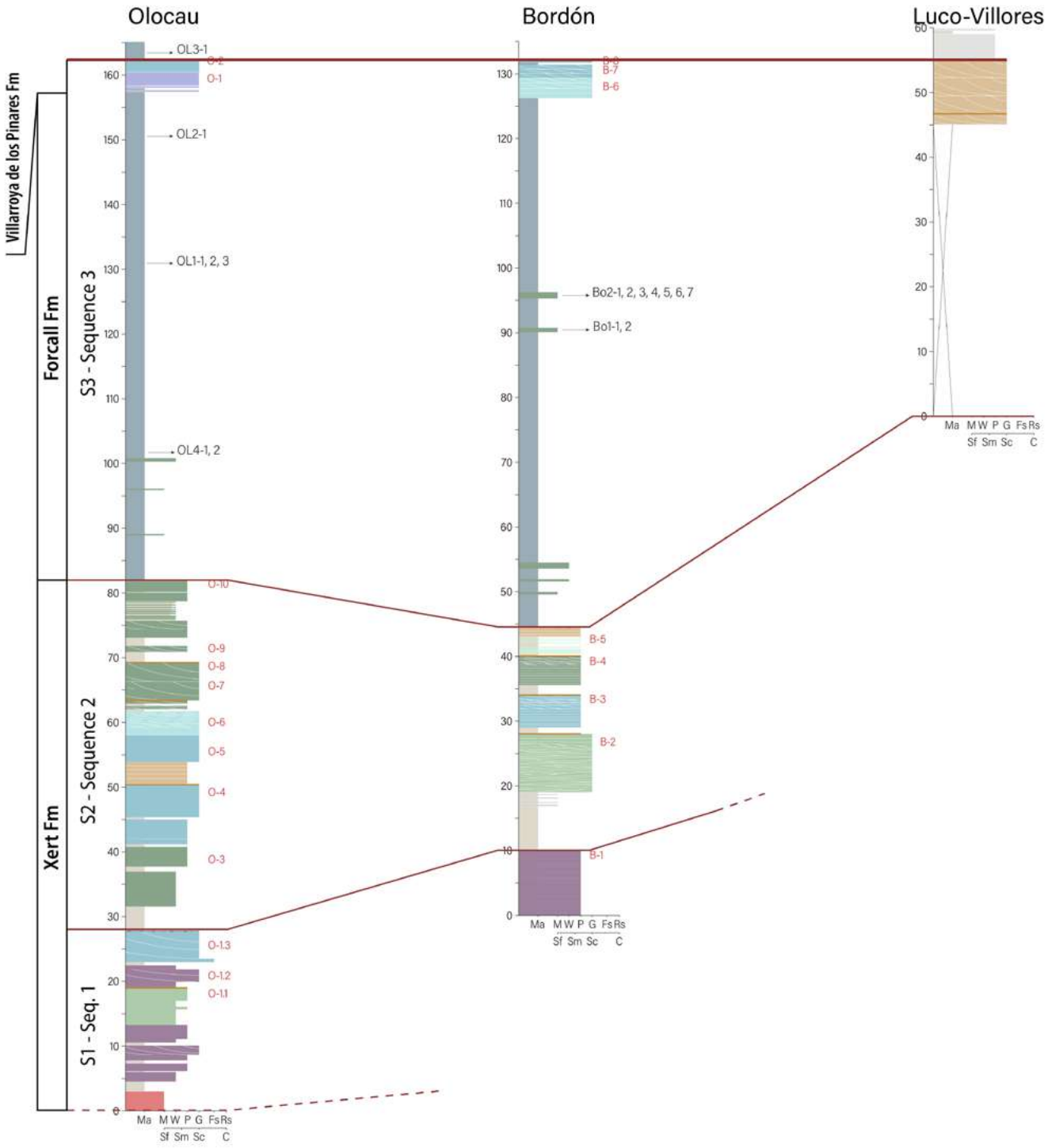

FIGURE VI.

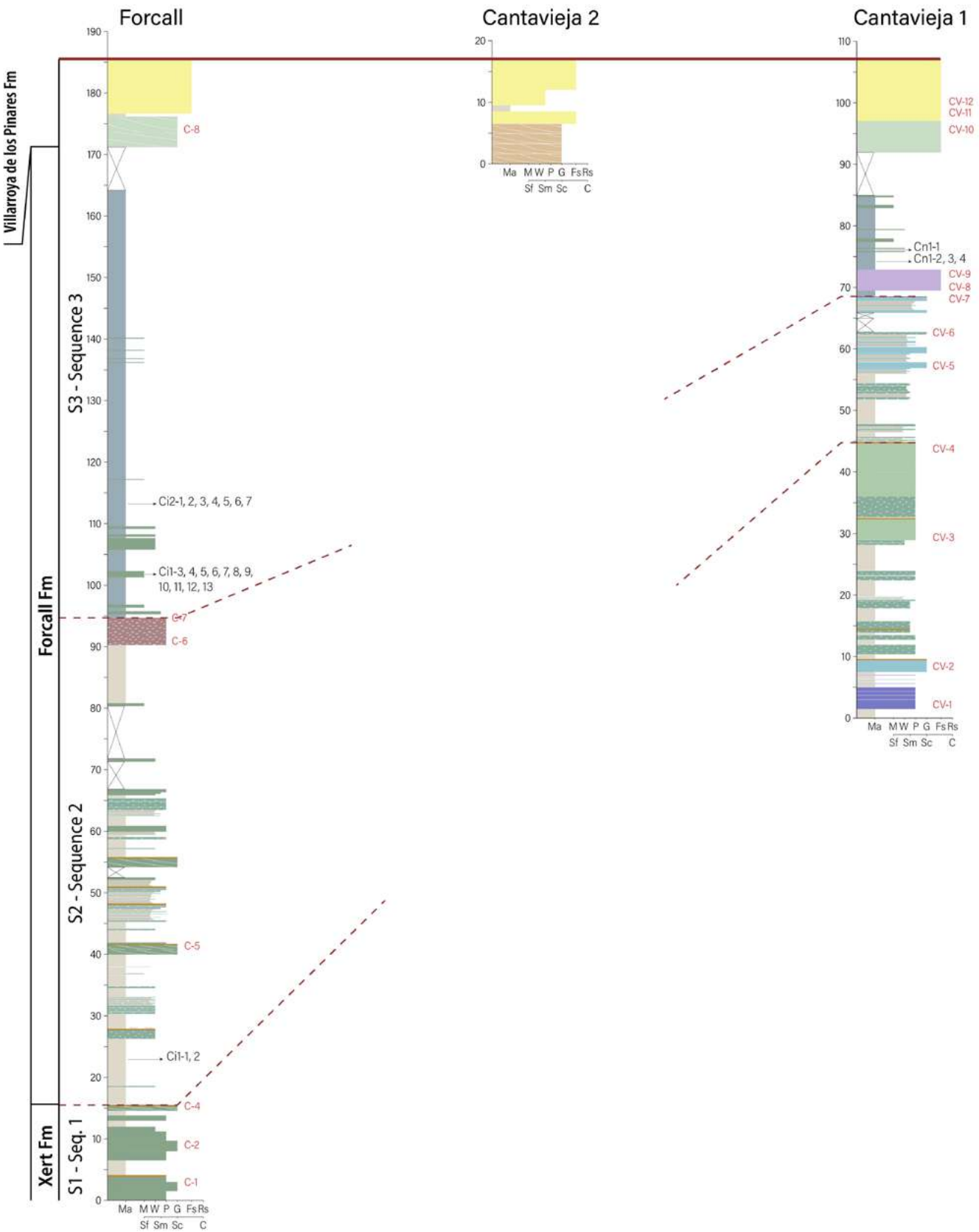
Forcall
Cantavieja 2
Cantavieja 1
Villarroya de los Pinares Fm
Forcall Fm
Xert Fm
S3 - Sequence 3
S2 - Sequence 2
S1 - Seq. 1
C-8
Ci2-1, 2, 3, 4, 5, 6, 7
Ci1-3, 4, 5, 6, 7, 8, 9, 10, 11, 12, 13
C-7
C-6
C-5
Ci1-1, 2
C-4
C-2
C-1
CV-12
CV-11
CV-10
Cn1-1
Cn1-2, 3, 4
CV-9
CV-8
CV-7
CV-6
CV-5
CV-4
CV-3
CV-2
CV-1
Ma M W P G Fs Rs
Sf Sm Sc C

FIGURE VII.

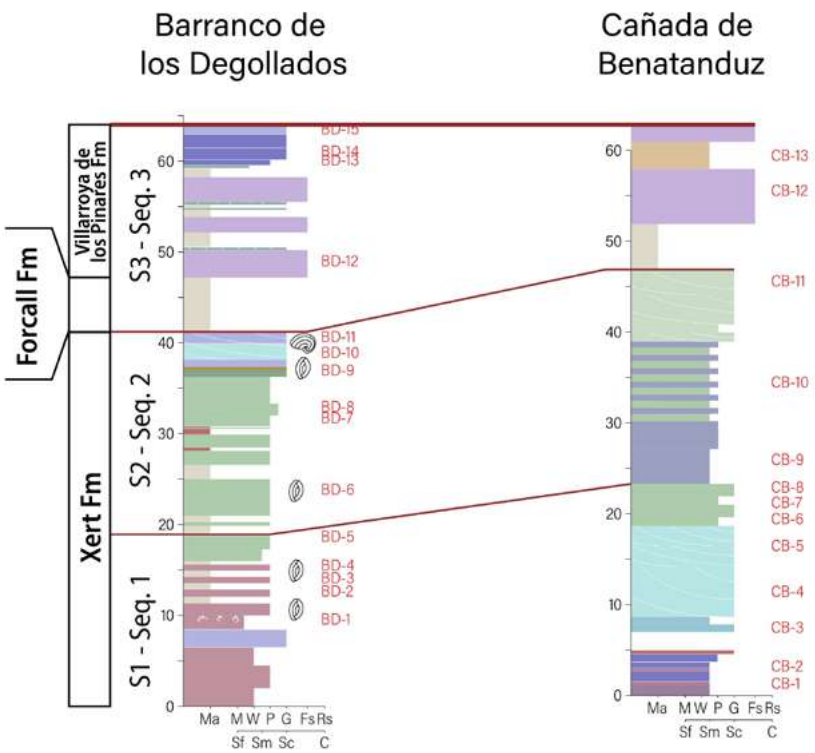

FIGURE VIII.